1-Reviewer Response:

We appreciate the thoughtful input from both of the reviewers, and we feel that we did address all the comments and suggestions that the reviewers have made on MS NO.:os-2016-4. Below, our point by point response is formatted as reviewer suggestion (**R**), author response (**AR**) and changes to manuscript (**MC**):

Reviewer #1

R1-1)"The underlying issue for this paper, determining if model fields can be used in the estimation of air-sea gas fluxes is interesting and important. However, I don't believe the present paper does a good job of answering the question posed. Rather than taking the output from the latest and most advanced ocean general circulation models, a number of which have been extensively evaluated in the Arctic, the authors try to set up and run their own coarse resolution simulations. Beyond some specific issues about the author's experiments and analysis, I don't see the purpose of these standalone experiments. Given the groups doing high resolution ocean modelling have the spent the time improving and evaluating their models, I don't see why such fields aren't being obtained and considered for this analysis. Additionally, since any given model has issues, doing this analysis with an ensemble of models would give much better confidence for the observational comparisons and thus the utility of numerical model output in calculating air-sea gas fluxes. "

AR-MC) The reviewer makes a valid point about model resolution. Initially, our goal was to use a model that could be run on a desktop, but since that time the resolution question has been recurring. Therefore, we have utilized other model resolutions, including model output from An. T. Nguyen (now a co-author and expert on MITgcm) and included those results in this revision. Hence on sections that we felt that 36km model does a poor job of following the data, we added 9km and 2km horizontal resolution.

It is apparent from these new model runs that increasing the resolution did not show improvements in its capacity to match the field data from moorings and ITP. We believe this discrepancy is due to input forcing of the model (ie reanalysis data products); specifically the low correlation in wind and air temperature reanalysis products on high frequencies which would make the accuracy of model invariant in respect to resolution.

R1-1)"Introduction: With the later focus on the Beaufort Gyre, it needs to be discussed (especially the observations that will later be used) in the introduction. The reader has otherwise no idea of the geographical focus until much later in the paper."

AR) We agree with R1 that the geographic boundaries of our comparison should be mentioned and we addressed it.

MC) Page 5 Paragraph 3:

"Most of the observed data exist in Beaufort Gyre, hence we mostly focus our comparison to that geographic perimeter. Figure 2 depicts the bathymetry and location of most important observations we used to make the comparisons with the model."

And Figure is added to the manuscript.

R1-2)"Page 3 Line 1: In areas of deep convection, the mixed layer can change by much more than a factor of 2 over several weeks."

AR) For the purpose of back tracing Radon-Labeled and gas exchange forcing acting upon it, time scale of interest is ~15-20 days, nevertheless we agree that it should be mentioned.

MC) Page 8 , line 4

"Between February and March, ITP-35 appears to drift through a zone of convection zone, likely caused by ice formation, with sudden increase of density near the surface. The same feature can be observed in both A1 and A2 density. However, on a smaller scale, there is significantly more variation in the ITP data than what the model represents."

R1-3)" Page 3, Line 17: Why do you need to use output from a model run on a desktop? Being able to run a model is a very different task compared to running a model to produce high quality evaluated output. Just take the fields from those produced by modelling groups."

AR) As stated above we added the 9km and 2km models which are extremely computational heavy models to our manuscript. Specifically we added 9km to mixed layer depth section and 9km and 2km models to water velocity section and removed "run on desktop".

MC) Page 4, Line 9

"Three ECCO's configurations are used, at horizontal grid spacings of 36 km, 9 km, and 2 km, respectively. The models are based on the Massachusetts Institute of Technology general circulation model (MITgcm) code and employ the z coordinate system described in Adcroft and Campin (2004). Our approach is first to assess the model outputs from the coarse resolu-

tion model using model-data misfits, then to investigate if there are quantitative reduction in model-data misfits with higher horizontal resolutions."

R1-3)"Page 4, line 14: Era40 is the output from an atmospheric reanalysis. This is not the same as a numerical weather forecast."

AR) The reviewer makes a very good point that we are not addressing the atmosphere products correctly, we fixed that.

MC) Page 4, line 13 "Surface forcings are from the 25 year Japanese Reanalysis Project (JRA25)(Onogi et al. 2007) for 36 km and 9 km runs and The European Center for Medium-Range Weather Forecasts (ECMWF) analysis for 2 km run"

R1-4)"Page 4, Line 19: Most high resolution models now use vertical resolution of 1-3 m near the surface."

AR) We removed the coarse resolution model with 10m vertical spacing from the figures and discussion and stated that our 36km and 9km share a 2m near surface vertical resolution and 2km model start with 1m vertical resolution near surface.

MC)Page 4 Line 23

"We introduced a set of new vertical grid spacings to allow us to capture near surface small details which cannot be represented with the coarser grid system. In the 36 km (hereafter referred to as A1) and 9 km (called A2) models, the spacing is 2 m in the upper 50 m of the water column and gradually increases to a maximum of 650 meters. In contrast, the 2 km model (called A3) has 25 layers in the top 100 meters of water column, starting from 1 meter and increasing to 15 meters step. "

R1-5) "Page 10, Line 8, etc.: Do not understand how the MLD could be zero. Model tracer points are in the middle of the grid cell for the MIT model. Thus, I don't see how the MLD could less than the depth of the first layer, given M1 is based on a threshold approach."

AR-MC) The zero mixed layer depth has been a byproduct of extrapolation of results from last grid point i.e. 1 meter below the surface to the surface. We agree with reviewer that such extrapolation is not necessary and we confined our analysis to first grid and removed any extrapolation. We also, in favor of limiting the number of figures, refrained to repeat our analysis for two methods of mixed layer calculation for ITP profiles and chose the M2 method for ITP mixed layer analysis. Aiming for consistency, we also changed the focused ITP from ITP-62 to ITP-V(35) for mixed layer depth discussion.

R1-6)" Page 10, line 11: Might it not be useful to use a simple 1-D mixed layer model to

examine directly the impact of the forcing."

AR) One definite advantage of coarse resolution model over the 1D model is the ability of coarse resolution model to produce sea ice advection. On 1D model the amount of sea ice on top of the water column is a function of heat budget. Ice that is formed on far field and moved by wind to top of the water column can affect the mixed layer and is neglected in 1D model.

To stress the importance of ice advection and ice openings by wind divergence and its effects on mixed layer change, we added a figure with 9km and 36km sea ice outputs on the path of ITP to mixed layer section and discussed the results.

MC) Figure 8 added, Page 9 Line 14

" The difference between A1 and A2 and their ability to capture MLD change, can be explained by the capability of a higher resolution model to capture small-scale fractures in the ice cover (Figure 8), and conversely, the inability of the coarser resolution to do so is due to averaging over a larger grid. The wind appears to be the primary driving mechanism for the divergence in ice cover, which in turn exposes the ocean to the cold atmosphere and lead to a loss of buoyancy and an increase in MLD. With higher resolution these openings can be captured, leading to a better agreement with data in marginal ice zones"

R1-7) Figures 26-32: I'm surprised the model and ITP velocities differ by so much. Have the model velocities been rotated from the model grid to latitude-longitude?

AR) We understand and shared the reviewers concerns over the accuracy of water velocity outputs. We checked and made sure that the velocities have been rotated and our rotation mechanism is sound, as seen by our sea ice velocity outputs. By comparing with higher resolution i.e. 2km and 9km, we made sure no improvement can be reached by increasing resolution either. We suspected and investigated the wind forcing. Chaudhuri et al. (2014) has published a comparison of all reanalysis products with data in Arctic and observed that none of the wind products has a correlation of more than 0.2. This low correlation propagates into water velocities.

We added 9km and 2km outputs to water velocity section and stated the effects of reanalysis wind products on near surface velocities. Also in favor of coherence, we limited our comparison to a single level for mooring data and a vertical average velocity between 5 to 50 meters for ITP-V data.

We also removed the subsection on Ekman analysis based on wind from water velocity section. Since we suspected the error to be originating from wind inputs, calculation of Ekman layer based on same wind was unnecessary.

MC) Figure 9 added ; Page 10 line 9

"We further add A3 to our comparison for moorings velocities (Figure 9), and compared velocities at 25m, which is the level that is shared between all our models and removes the necessity of any interpolation. The simulation results show RMSE normalized by data of higher than 5 and correlations of less than 0.3 over 3 moorings and almost two years of data. This result indicates ocean currents are not well captured in the model irrespective of horizontal grid resolution. We must therefore look into the atmospheric forcing as a likely source of error on high frequency water velocities near surface. As noted above, the wind inputs into the model from the reanalyses are available at frequency 6-hourly. (Chaudhuri et al. 2014; Lindsay et al. 2014) have compared various available reanalysis products over the Arctic which we used to force our model, along with multiple other reanalysis products with available ship-based and weather station data and found out that wind products in all of those have low correlation i.e less than 0.2. To investigate we compared Jra55 and NCEP to a shipboard data gathered during 2014 in time span of 2 months in Arctic and found that JRA55 had -0.20 correlation, RMSE of 7.36 and bias of -1.3, NCEP had correlation of 0.10, RMSE of 5.73 and bias of -1.40 when compared with high frequency data on each cruise, reinforcing our suspicion of high frequency wind as a source of error in water currents."

Reviewer #2

R2-1)"The motivation of the paper is to estimate the mixed layer depth from the ocean model; however, the following sections do not seem to have any connections to the mixed layer depth estimation: 3.3.1 Geopotential height, 3.31 Vertical salinity temperature profiles and 3.6 Circulation and etc. This makes the interpretation of this paper difficult and results in many figures, which are not labeled correctly. For example, line 20 describes the sea-ice trajectory, but Fig. 10 contains color plot of geopotential and arrows, which are not described. Line 25 describes the geopotential, yet the referred figure 12 does not contain any information on the geopotential. I would keep the section 3.5 Mixed layer depth and omit 3.3.1, 3.6 and 3.7 unless there are clear connections to the change in the mixed layer depth."

AR) We agree with the reviewer that some sections needed to be removed and we also needed to state our hypothesis and aims more clearly. We edited the introduction to clearly state our target from the start and we removed the "geopotential height" and "general circulation" sections from manuscript. We also added a section where we calculate gas exchange on 3 grid points based on model outputs to demonstrate the impact of kept sections on gas exchange.

MC:Section "geopotential height" and "general circulation" are removed, Section 4 "Gas exchange estimation" is added.

Page 2 Line 14

"Lacking sufficient data to constrain these processes, we wonder whether it is possible for a numerical model to adequately capture forcing of air-sea gas exchange in the sea ice zone and consequently improve predictions of air-sea flux. The parameters of interest are sea ice concentration (or fraction of open water), sea ice velocity, mixed layer depth, and water current

speed and direction in the ice-ocean boundary layer (IOBL) (Loose et al. 2014). Here we use the budget of ^{222}Rn gas in the IOBL as an example, because the radon-deficit method has emerged as on of the principle methods to estimate k in ice-covered waters (Rutgers Van Der Loeff et al. 2014; Loose et al. 2016)."

R2-2)"The paper claims in the abstract "Overall, we find the course resolution model to be an inadequate surrogate for sparse data, however the simulation results are a slight improvement over several of the simplifying assumptions that are often made when surface ocean geochemistry, including the use of a constant mixed layer depth and a velocity profile that is purely wind-driven." I agree with the first claim "find the course resolution model to be an inadequate surrogate for sparse data"; however I do not see where the second claim, "the simulation results are a slight improvement over several of the simplifying assumptions that are often made when surface ocean geochemistry", is supported in the paper. The authors need to show the rate of air-sea gas exchange calculated from the mixed layer depth from 1) the ocean model results and 2) the conventional method, and discuss the difference in the estimates."

AR-MC) To demonstrate each parameter we calculated in our manuscript, we added section 4 Gas exchange estimation

MC)Section : 4 - Gas exchange estimation and Figure 10 added.

R2-3)"I am concerned with the use of salt plume parameterization in the model configuration, A1. The A1 has relatively high vertical resolution of 2 m down to upper 50 m, whereas the salt plume parameterization is tested for models having the vertical resolution of _10 m. The salt plume parameterization is known to suppress the mixing to maintain a reasonable mixed layer depth in the polar regions. The parameterization is meant for a coarse vertical resolution model (_10 m). The vertical resolution in A1 is 5 times higher, and I am concerned that the parameterization in A1 is over suppressing the mixed layer depth. In fact, Figs 11, 13 20, 21 all points to the underestimation of the mixed layer depth compared to the observations. I suggest switching off the salt plume parameterization and evaluating the mixed layer depth in comparison to the existing model results and observations."

AR) After we noticed the reviewers concern with salt plume parameterization, we preformed a series of 1D-tests with and without the scheme and found no dependency of this scheme on vertical resolution. We also compared mixed layer from A3 (no salt plume) to A1 and A2 (salt plume) and confirmed that this parametrization is not responsible for mixed layer bias.

MC) Page 9 Line 24

"One last important note is the effect of the salt plume parameterization (SPP) on MLD. Nguyen et al. (2009) demonstrated the need to remove the artificial excessive vertical mixing in coarse horizontal resolution models. To rule out the dependency of this parametrization to vertical resolution as a source in MLD bias, we preformed a suit of 1D tests, with and without the SPP on variety of vertical resolutions (not shown here) and sea ice melting/freezing scenarios and confirmed that SPP is not dependent on vertical grid spacing. We also investigated MLD in A3 (no SPP) run compared to A2, and confirmed the average MLD is the same between these 2 runs."

Minor Comments

"Line 10-15: It is unclear if the lateral boundary conditions are prescribed from the climatology or seasonal output from ECCO2 and JRA25. It is also unclear why the authors use output from two different models ECCO2 and JRA25. Map of the domain showing bathymetry will be helpful."

AR) Thanks you. We changed the text to clarify that our boundary conditions are from ECCO2 and surface forcing on the domain is from JRA25.

MC) Page 4 Line 13

Surface forcings are from the 25 year Japanese Reanalysis Project (JRA25)(Onogi et al. 2007) for 36 km and 9 km runs and The European Center for Medium-Range Weather Forecasts (ECMWF) analysis for 2 km run.

Page 4 Line 19

The horizontal boundary condition for the 36 km and 9 km configurations comes from existing global ECCO2 model outputs (Marshall et al. 1997; Menemenlis et al. 2008; Losch et al. 2010; Heimbach et al. 2010).

"Equation 3: What is the definition of i?"

MC)this section has been removed as part of R1-7.

2-Changes Marked in Manuscript :

Numerical investigation of the Arctic ice-ocean boundary layer; implications for air-sea gas fluxes

A. Bigdeli[1], B. Loose[1],An T Nguyen[2], S. T. ~~Cole~~[2]Cole[3]

[1]Graduate School of Oceanography, University of Rhode Island, Rhode Island, 02882, U.S.A
~~[2]Woods~~[2]University of Texas at Austin, Austin, Texas, 78712, US
[3]Woods Hole Oceanographic Institution, Woods Hole, Massachusetts, 02543, U.S.A

Correspondence to: A.Bigdeli (Arash_Bigdeli@uri.edu)

Abstract. In ice-covered regions it ~~can be~~is challenging to determine ~~air-sea exchange~~constituent budgets – for heat and momentum, but also for biologically and climatically active gases like carbon dioxide and methane. The harsh environment and relative data scarcity make it difficult to characterize even the physical properties of the ocean surface. Here, we seek to evaluate if a ~~mechanistic interpretation for~~ numerical model output helps us to better estimate the ~~rate of~~ physical forcing that drives the air-sea gas exchange rate (k) ~~derived from radon-deficits. These require an estimate~~ in sea ice zones. We use the budget of radioactive ^{222}Rn in the mixed layer to illustrate the effect that sea ice forcing has on gas budgets and air-sea gas exchange. Appropriate constrain of the ^{222}Rn budget requires estimates of sea ice velocity, concentration, mixed layer depth, and water ~~column history extending 30 days prior to sampling.~~velocities, as well as their evolution in time and space along the lagrangian drift track of a mixed layer water parcel. We used ~~coarse~~36 km, 9 km and 2 km horizontal resolution ~~(36km)~~of regional configuration of ~~the~~ MITgcm with fine ~~near surface~~ vertical spacing ~~(2m)~~ to evaluate the capability of the model to reproduce ~~conditions prior to sampling. The model is used to estimate sea-ice velocity, concentration and mixed-layer depth experienced by the water column~~these parameters. We then compared the model results to existing field data including satellite, moorings and Ice-tethered profilers. We found that ~~model-derived~~ mode sea-ice coverage ~~is~~agrees with satellite-derived observation 88 to 98% ~~accurate~~of the time when averaged over the Beaufort Gyre, and model sea-ice ~~velocities~~speeds have ~~78~~82% correlation ~~which resulted in 2 km/day error in 30 day trajectory of sea-ice~~with observations. The model demonstrated the capacity to capture the broad trends in the mixed layer although with a significant bias ~~and model~~. Model water velocities showed only 29% correlation with ~~actual~~point-wise in situ data. This correlation remains low in all three model resolution simulations and we argued that is largely due to the quality of the input atmospheric forcing. Overall, we ~~find~~found that even the ~~course~~coarse resolution model ~~to be an inadequate surrogate for sparse data, however the simulation results are a slight improvement over several of the simplifying assumptions that are often made when surface ocean geochemistry~~can make modest contribute to gas exchange parameterization, by resolving the time variation of

parameters that drive ^{222}Rn budget, including ~~the use~~rate of ~~a constant~~ mixed layer ~~depth~~change and ~~a velocity profile that is purely wind-driven~~sea ice forcings.

1 Introduction

The ocean surface is a dynamic region where momentum, heat and salt, as well as biogeochemical compounds are exchanged with the atmosphere and with the deep ocean. ~~These fluxes drive vertical mixing that generates the mixed layer. On the top of the mixed layer, at~~At the sea-air interface, gases of biogenic origin and geochemical significance are exchanged with the atmosphere. Theory indicates that the aqueous viscous sublayer, which has a length scale of 20 to 200 µm~~,~~ (Jähne and Haubecker 1998~~))~~, is the primary bottleneck for air-water exchange. Limitations in measurement at this critical scale have led to approximations of sea-air gas exchange based on indirect measurements. Four approaches involving data are typically used (Bender et al. 2011), 1) Parametrization of the turbulent kinetic energy (TKE) at the base of the viscous sublayer 2) Tracing purposefully injected gases (Ho et al. 2006; Nightingale et al. ~~2000~~2000a) 3) Micro Meteorological methods (H. J. Zemmelink et al. ~~2006,~~2006a; Zemmelink et al. 2008; Blomquist et al. 2010; Salter et al. 2011), and 4) Radon-deficit Method. Here, we examine the radon-deficit method (4), together with a parameterization of the TKE forcing (1) that theoretically leads to the observed deficit in mixed-layer radon.

When the ocean surface is not restricted by fetch, TKE is mostly dominated by wind speed ~~on open ocean interface~~and waves (Wanninkhof 1992; ~~Ho~~H. J. Zemmelink et al. ~~2006~~2006b; Wanninkhof and McGillis 1999; Nightingale et al. ~~2000~~2000b; Sweeney et al. 2007; Takahashi et al. 2009). In the polar oceans wind energy and atmospheric forcing are transferred in a more complex manner as a result of sea ice cover (Loose et al. 2009, 2014; Legge et al. 2015). Sea ice drift due to Ekman flow (McPhee and Martinson 1992), freezing and melting of ice leads on the surface ocean (Morison et al. 1992) and short period waves (Wadhams et al. 1986; Kohout and Meylan 2008) all constitute important sources of momentum transfer. Considering the scarcity of data on marginally covered sea-ice zones (Johnson et al. 2007; Gerdes and KöBerle 2007), especially during ~~arctic~~Arctic winter time, ~~comparing and validating~~the environment is too poorly sampled to constrain these ~~models are quite challenging.~~ processes through direct measurement or empirical relationships.

~~The radon~~Lacking sufficient data to constrain these processes, we wonder whether it is possible for a numerical model to adequately capture forcing of air-sea gas exchange in the sea ice zone and consequently improve predictions of air-sea flux. The parameters of interest are sea ice concentration (or fraction of open water), sea ice velocity, mixed layer depth, and water current speed and direction in the ice-ocean boundary layer (IOBL) (Loose et al. 2014). Here we use the budget of ^{222}Rn gas in the IOBL as an example, because the radon-deficit method has emerged as on of the principle methods to estimate k in ice-covered waters (Rutgers Van Der Loeff et al. 2014; Loose et al. 2016).

The Radon deficit method involves sampling ^{222}Rn and ^{226}Ra in the mixed layer to examine any difference in the concentration or (radio) activity of the two species. Radon is a gas, radium is a cation; in absence of gas exchange ^{222}Rn and

^{226}Ra enter secular equilibrium meaning the amount of ^{222}Rn produced is equal to decay rate of ^{226}Ra. Any missing ^{222}Rn in the mixed layer is attributed to exchange with atmosphere (Peng et al. 1979).

Since the ^{222}Rn concentration in air is very low, less than 5% (Smethie et al. 1985) and considering that concentration is proportional to activity/decay rate A, we can use Eq. (1) to determine gas exchange. Where k gas transfer velocity in (m d-1), A_E is the activity or decay rate of ^{222}Rn which in secular equilibrium is equal to ^{226}Ra activity, A_M is ^{222}Rn measured decay rate in mixed layer, λ is decay constant of ^{222}Rn (0.181 d-1) and h is the mixed layer depth

$$k = [A_E / A_M - 1]\lambda h \quad (1)$$

The mixed layer depth, h, is calculated from the measurements performed at the hydrographic stations during ^{222}Rn sampling process.

~~(1)~~

Gas transfer velocities from equation (1) reflect the memory of ^{222}Rn for a period of two to four weeks (Bender et al. 2011), which is four to eight times the half-life of ^{222}Rn (3.8 days). ~~The mixed layer depth, h, is calculated from the measurements performed at the hydrographic stations during ^{222}Rn sampling process.~~

~~While a valuable tool this method is based on two premises, a) an invariant~~This memory integrates the physical oceanography properties of the IOBL, including sea ice cover, mixed layer depth and ~~b) invariant TKE forcing~~water current speed are likely to vary significantly during ~~the entire~~this period ~~of "memory" that gas~~and it is important to consider these processes as a source of uncertainty in ~~the mixed-layer has experienced.~~Eq. (1). To ~~further~~ illustrate ~~the discrepancy caused by utilizing the invariant assumptions, described above~~this uncertainty, consider a mixed layer that rapidly changes by a factor of 2 just prior to sampling for radon. If the mixed-layer becomes shallower ~~(~~by stratification~~)~~, h ~~– defined by the density profile -~~ will be smaller by factor of 0.5 while A_E/A_M in the mixed layer remains the same. Based on equation 1, this causes k to be half of its true value. That is, prior to stratification TKE forcing was sufficient to ventilate the ocean to a depth greater than the apparent h (Bender et al. 2011).

Conversely, if the mixed layer deepens due to mixing, h increases and a new parcel of water with A_E/A_M= 1 is added to mixed layer, causing the activity ratio to come closer to unity. These two influences on equation 1 (increasing H and A_E/A_M approaching unity) work against each other, but the net effect is to cause k to appear larger. The change of factor of 2 or higher (in case of convection) in mixed layer depth in less than two weeks has been observed during several studies (Acreman and Jeffery 2007; Ohno et al. 2008; Kara 2003).

The "memory" of gas exchange forcing that radon experiences is further complicated by the presence of sea ice. Consider two alternate water parcel drift paths that lead to the ^{222}Rn sampling station in sea-ice zone (~~Fig.~~Figure 1). Path B demonstrates a history which water column spends most its back trajectory under sea-ice. Path "A" shows a water column

which experiences stratification and ~~shallowing~~shoaling of mixed layer depth equal to δh when drifting through water that is completely uncovered by ice. During most of Path "B" gas transfer happens in form of diffusion through sea-ice and it will have a very low k (Crabeck et al. 2014; Loose et al. 2011~~). In~~), in contrast Path "A" will have a greater radon deficit, but a smaller h because of stratification. In either case, it is critical to take into account the time history of gas exchange forcing, including changes in the mixed-layer and ice cover, which has led to the apparent radon deficit at the time of measurement.

This observation about drift paths in the sea ice zone strongly implies that we must consider both time and space in estimating the forcing conditions that are recorded in the radon deficit. In other words, we require a Lagrangian back trajectory of water parcels to track the evolution of mixed layer and its relative velocity 4 weeks prior to sampling.

Although satellite data, Ice tethered drifters (Krishfield et al. 2008) and moorings (Krishfield et al. 2014; Proshutinsky et al. 2009) have provided valuable seasonal and spatial information about the sea ice zone, they do not track individual water parcels and tend to convolve space and time variations. The spatial limitation of these data ~~pose~~poses a challenge to producing a ~~a~~ back trajectory of the water parcel ~~hence we used a 3D numerical model to simulate these data~~.

~~This is~~To address the ~~principle goal of our study –~~above mentioned challenges, we ~~want~~use a suit of the Estimation of the Circulation and Climate of the Ocean (ECCO) project's Arctic regional configurations to ~~know~~test the if a ~~coarse resolution~~ numerical model ~~that~~ can be ~~run on a desktop multi-core processor can provide us with spatial and temporal information to better model~~ used to follow the back trajectory of a radon-labelled water parcel~~. The null hypothesis might therefore be, that simple assumptions such as an invariant~~ and the gas exchange forcing acting upon it and yield the missing information required for the Radon deficit method.

The variables and derived quantities of interest from the numerical model include mixed~~-~~ layer~~, Ekman ice drift and area-averaging of~~ depth (MLD), sea ice ~~cover are as good or better at reproducing the radon-based estimates of k.~~

~~We set up a numerical simulation that captures near surface phenomena as a means to access the history of a~~ concentration and speed (Loose et al. 2014) and the water ~~parcel sampled for radon, and the forcing conditions that led to the observed radon deficit. For this study we are focusing on near surface phenomena~~ velocity in the ~~Arctic using the Arctic Regional configuration of the MITgcm with the domain of ECCO2 (Marshall et al.~~ MLD. We note that~~1997; Menemenlis et al. 2008; Losch et al. 2010; Heimbach et al. 2010; Nguyen et al. 2011). A number of Arctic ocean-ice models which have been compared~~ as part of Arctic Ocean Models Intercomparison Project (AOMIP~~)~~), a number of Arctic ocean-ice models' capability to represent main ice-ocean dynamics s have been assessed (Proshutinsky et al. 2001; Lindsay and Rothrock 1995, p. 995; Proshutinsky et al. ~~2008) in regard to their capability to represent main ice-ocean dynamics. This model has shown to have better~~ 2008). Our reasons for choosing ECCO over other Arctic models stem from the higher correlation ~~with remotely sensed~~between the ECCO's regional Arctic simulated outputs to satellite derived sea ice data (Johnson et al. 2012) and the feasibility in the MITgcm to adapt a high near surface vertical resolution to existing configurations.

~~It is worth noting that model studies using higher resolution evaluate model skill are already in print. For example, Holloway et al., (2011) use a 4 (km) version of the MITgcm regional model has a high skill in producing near surface velocities and capturing eddies. So, the choice to use the 36 (km) resolution model may seem anachronistic. However, we~~

~~approach this problem as geochemists who are searching for a data interpretation tool. We seek higher resolution in the top 100 m of the water column, as compared to these prior studies. Furthermore, the 36 (km) model can be run on a desktop multi-core processor, and the simulation is completed in less than a week.~~

The remainder of the article is organized as follows: In section 2 we ~~introduce~~ provide the details of the ~~changes we made to increase the near surface resolution.~~ECCO ice-ocean models. Section 3.1 and 3.2 ~~contain the comparison of the new results and original~~focus on model outputs ~~including~~of sea-ice concentration~~;~~ and velocity and ~~trajectory to observed data~~comparison with observations from satellite and Ice tethered ~~profiler. Sections~~profilers. Section 3.3~~, 3.4 and 3.5 are used to study~~ investigates the ~~model~~modeled output salinity and temperature structure and the resulting upper ocean density structure and mixed layer. ~~Sections 3.6 and 3.7 evaluate the qualitative model circulation and~~Section 3.4 evaluates the correlation in near surface water velocity. ~~Lastly, section 4 shows~~In section 4 we discuss the results and sources of error and their impact on estimated gas exchange and lastly, section 5 provides the summary of our results. ~~In each section, we attempt to compare model output to direct observations, and to simple assumptions – such as those that are commonly made in geochemical studies of the upper ocean. These comparisons help define the relative value of the model output to geochemical data interpretation.~~

2 Method

~~The~~2.1 ECCO model ~~has a~~ configurations

Three ECCO's configurations are used, at horizontal ~~resolution~~ grid spacings of ~~36km~~36 km, 9 km, and ~~50 vertical layers employing~~2 km, respectively. The models are based on the Massachusetts Institute of Technology general circulation model (MITgcm) code and employ the z~~*~~ coordinate system ~~(~~described in Adcroft and Campin ~~2004) and the maximum model depth of 6150m. The surface forcing is soureed from ERA40 and ECMWF numerical weather forecast, and the boundary conditions are taken~~(2004). Our approach is first to assess the model outputs from the coarse resolution model using model-data misfits, then to investigate if there are quantitative reduction in model-data misfits with higher horizontal resolutions. Surface forcings are from ~~output of the ECCO2 global model (Menemenlis et al. 2008) and~~the 25 year Japanese Reanalysis Project (JRA25)(Onogi et al. ~~2007).~~2007) for 36 km and 9 km runs and The European Center for Medium-Range Weather Forecasts (ECMWF) analysis for 2 km run. Initial conditions are from World Ocean Atlas 2005 (Antonov et al.; Locarnini et al.) and initial sea ice conditions are from (Zhang and Rothrock 2003~~), model is~~) for the of 36 and 9 km, from which the models are allowed to spin up from ~~1979 to 1992.~~1992. The 2 km global run is initialized from a 4 km spin up version of the ECCO adjoint-based state-estimate for Jan 2011 and covers the period Feb 2011 to Oct 2012. The vertical mixing uses K profile parameterization (KPP) developed by (Large et al. ~~(~~1994) and 36 and 9 km runs utilize salt plume parameterization of Nguyen et. al(2009). The horizontal boundary condition for the 36 km and 9 km configurations comes from existing global ECCO2 model outputs (Marshall et al. 1997; Menemenlis et al. 2008; Losch et al. 2010; Heimbach et al. ~~al. (2009~~2010).

We introduced a set of new vertical grid ~~spacing~~ spacings to allow us to capture near surface small details which cannot be represented with the coarser grid system. In the 36 km (hereafter referred to as A1~~), 2~~) and 9 km (called A2) models, the spacing is 2 m in the upper 50 m of the water column and gradually increases to a maximum of 650 meters. In contrast, the 2 km model (called A3) has 25 layers in the top 100 meters of water column, starting from 1 meter ~~steps near surface which continue to the depth of 50 meter which then gradually increase to a maximum interval of 650 meters in deep ocean contrasting to the optimized model (called A0) which had 10 meter intervals near surface, progressively~~and increasing to ~~450 meter at maximum depth.~~15 meters step. All the boundary conditions from ECCO2 have been interpolated to match the new ~~grid system. Due to stability condition of the model we also reduced the time steps of the model from 2400 seconds to 600 seconds. The model simulates the time period from January 1992 to September 2013. This new grid system allows us to capture near surface small details which cannot be represented with the coarser grid system.~~ vertical grid system.

2.2 Observations

Satellite-derived estimation of sea-ice cover at 25km horizontal resolution (Comiso 2000) is ~~being~~ interpolated ~~on~~to a horizontal grid system ~~and then compared with A0 and A1. Then~~to facilitate model-data comparison. In addition, sea-ice drift gathered by 28 Ice Tethered Profilers (ITP) (Krishfield et al. 2008) which has more than 2 ~~month~~months of data in Beaufort Sea between 2006 and 2013 has been used to do the ice velocity ~~and trajectory~~ comparison~~. We selected only ITPs with 2 or more months of drift data in the Beaufort Sea~~.

We compared near surface water velocity data from ITP-V (Williams et al. 2010) to A1 and A2 and upward looking Acoustic Doppler Current Profiler installed on McLane Moored Profiler (MMP) (~~Proshutinsky~~McPhee et al. 2009; ~~Krishfield~~Cole et al. 2014) to A1,A2 and A3 in order to compute the accuracy and feasibility of calculating back trajectory of parcels located at the mixed layer. We limit our comparison of ITP-V which runs from Oct-2009 to Mar-2010 to A1 and A2 since those models run from 2006 to 2013 and A3 runs from 2011 to 2013.

Using salinity and temperature profiles from ITPs (Krishfield et al. 2008) we calculated mixed layer depth and ~~the average geopotential height between 2006 and 2013 and~~ compared it to 2m vertical resolution model output (A1~~).~~,A2). Most of the observed data exist in Beaufort Gyre, hence we mostly focus our comparison to that geographic perimeter. Figure 2 depicts the bathymetry and location of most important observations we used to make the comparisons with the model.

3 Results

3.1 Sea ice concentration

~~**Both A0 and A1 model scenarios are used to study sea ice extent (area of cells with more than 15% ice cover) from 1992-2013. At the Arctic Basin scale, the model depicts a decrease in the September minimum sea ice extent of 0.82 million square kilometres per decade or 10% of the starting value at 1992 compared to satellite data which display a 1.2 million square kilometres per decade, the model show an over estimation of sea-ice extent (Fig. 2). For further** For Sea ice concentration **analysis we introduced a grid system covering the Beaufort Gyre and interpolated the data from satellite (Comiso 2008) and ~~A0 and~~ A1 on to the grid.**

The analysis grid extends from 70° to 80° north and 130° to 170° west, covering most of Beaufort Gyre ~~(Fig.~~Figure 3~~).~~. Grid points can be divided into two main geographic zones that are marked out based on sea ice cover. The first zone contains grid points where the annual average sea ice cover is greater than 80%. These sets of points are fully covered by sea-ice most of the year. The second zone can be described as "marginally ice covered" wherein the ocean surface is free of ice for some fraction of the year. We chose 3 points within this sea ice geography to compare the seasonal and interannual behavior of the model with satellite ice cover. The points are located at 80~~°~~, N,131.82° W (P1), 70.82° N 169.82° W(P2), and 74.76° ~~north~~N and 163.51° ~~west~~W (P3).

The ice cover at P1, P2 and P3 ~~(Fig. 4)~~Figure 3 can be divided into 3 ice phases: (a) Fully covered in ice, (b) Open water and (c) a transition between (a) and (b). P3, which is the furthest south, has all three phases. In contrast P1 ice cover only dips below 60% for two brief periods during the 7 year time series depicted in Fig 4 - once in 2008 and again in 2012. These three points illustrate where and when the model has the greatest challenge reproducing the actual sea ice cover. At the extremities of the ice pack, where the water is predominantly covered by 100% or 0% ice (P1 and P3), the model captures the seasonal advance and retreat and the percent ice cover itself is accurate. However, in the transition regions that are characterized by marginal ice for much of the year (P2), the model has more difficulty reproducing ~~accurate~~the observed sea ice cover as well as the timing of the advance and retreat. ~~These results are the same for both A0 and A1 experiments, and this~~This behavior is consistent with the description that has been explained by Johnson et al. (2007), that models have a higher accuracy predicting sea ice concentration in central ~~arctic~~Arctic and less accuracy near periphery and lower latitudes.

The spatial sensitivity of the model can be observed using root mean square (RMS) error Eq. (2), calculated over the 1992-2013 period ~~(Fig. 5).~~Figure 3. The area with ~~most error~~the highest misfits coincides with area between the 80% and 60% contour lines ~~(Fig.~~Figure 3~~)~~ and is concentrated primarily in the Western Beaufort. The RMSE error of 0.2 is the maximum value away from land, this same level of error can also be found near land which is caused by fast-ice generation. Fast Ice in the model is replaced with pack of drifting sea ice; this error is common ~~between~~among numerical models and has been ~~studied~~brought to attention during AOMIP (Johnson et al. 2012~~, p. 20~~).

~~,~~ ~~(2)~~

$$RMSE(point) = \sqrt{\sum_{i=1}^{n} (C_{simulation} - C_{satellite})^2 / n} \quad (2)$$

If we compare the monthly climatology for sea ice cover over the 1992-2013 period, the RMS error between model and satellite data is least during the early winter months (e.g. Jan-Mar) when sea ice is close to its maximum extent. Comparing ~~A0~~Data and A1 ~~Fig. 5~~Figure 3 depicts an increase in RMSE during July, August, September and October and a minor decrease in May and November. The RMSE appears to be greater during the summer months of ice retreat, and slightly less during the autumn months of ice advance. Overall, the periods of transition (melt and freeze) coincide with the greatest RMSE.

~~The 2m revised grid (A1), with smaller vertical intervals near the surface has produced a greater RMSE than the optimized model (A0). We are still exploring why this took place. It is possible that the convective parameterization in the ice model is somehow negatively affected by short i.e. 2 m vertical layers. To reproduce changes in the mixed layer will require the greater resolution reflected in the A1 model run.~~

An important source of errors in the model ice concentration comes from the reanalysis surface forcing. Fenty and Heimbach (2012) showed that adjustments in the air temperature that are within the uncertainties of this reanalysis field can help bring the model ice edge into agreement with the observations. Of note also is that the uncertainty in satellite-derived ice cover can be the highest in the marginal ice zone due to tracking algorithms that are sensitive to cloud liquid water or can not distinguish thin ice from open water (Ivanova et al. 2015), this error also manifest itself in quantification of model-data misfits.

3.2 Sea ice velocity ~~and trajectory~~

Ekman turning causes ice and water to move at divergent angles with respect to each other. Ice moves the fastest, with mean values of 0.09 m s^{-1} (Cole et al. 2014), and the water column progressively winds down in velocity, along the Ekman spiral. Stratification in the Arctic leads to a confinement of the shear stress closer to the air-sea interface and also produces greater divergent flow vectors between ice and water (McPhee 2012). In the marginal ice zone or in regions where ice is converging or diverging, these motions, relative to the motion of the water column can produce significant changes in the water column momentum budget as well as air-sea fluxes. Thankfully, the ITPs can provide us with a measure of the real ice drift.

~~For purposes of comparison with the model and ITP drifts estimated a simple sea-ice velocity vector field Eq. (3) using reanalysis wind data (Onogi et al. 2007), with "a" and θ as empirical coefficients equal to 0.019 and 28 degree (Cole et al. 2014), This simple estimation neglects feedback from Ekman spiral under the ice which has been implemented in more sophisticated analytical solutions (Park and Stewart 2015).~~

~~, (3)~~

To generate a more quantitative comparison between the results we utilized the same method ~~used~~introduced by Timmermans et al. (2011), ~~comparing~~to compare ice velocity components (~~u-v~~eastward - northward) of ~~A0,~~ A1 ~~and estimated velocity from Eq. (3)~~ to ITP velocity and ~~finding~~compute the correlation coefficient of each experiment ~~versus~~with the daily averaged actual drift velocity ~~of~~from the ITPs ~~(Fig. 6)~~Figure 4).

~~By averaging~~ When averaged over all the ITPs operating in Beaufort Gyre during 2006 to 2013, ~~A0~~A1 had ~~0.78, A1 0.77 and simple estimation had 0.65 correlation with~~ correlations of 0.8 with actual velocity components~~.~~

~~As stated in the introduction, one of the principle objectives of this study is to evaluate the capability of the MITgcm to produce useful forcing field on the time-scale of mixed layer memory for biological and geochemical compounds, particularly the volatile ones. For a trace gas such as oxygen or radon, we only require adequate representation of the time-history of hydrographic conditions that act upon on a tracer for ~30 days, because this is the approximate renewal time of the mixed layer, based on a representative value of air-sea exchange. Consequently, we need the ice that covers our Lagrangian water parcel, so we calculated 30 day trajectories of sea-ice. We generated the ice floe trajectories by step-wise integration of the daily-average ice model output of velocity and direction in order to follow the individual ice floe. To illustrate, we have selected one of the 28 ITPs - ITP53 during its operation in Beaufort Sea from August 6, 2011 to August 13, 2012.~~

~~To generate a statistically large sample size, this calculation is preformed such that every day is treated as a starting point for simulation and the trajectory of that parcel is traced for a 30 day period. Figure 7 shows the result of this calculation for ITP 53. Taking the separation between the actual ITP trajectory after 30 days and the model trajectory, we determine the average drift error. Using 28 ITPs and 11744 operation days, for a total of N = 352320 data points. The average separation is 59.3 (km) for A0 and 62.5 (km) for A1 that is equal to 1.97 and 2.08 (km/day) error respectively. This amounts to a 5% increase in the error from A0 to A1. Same calculation for trajectories based on Ekman drift sea-ice velocities computed from Eq. (3) yield 4.3 km/day error. In other words, the coarse resolution model error is approximately half as large as if we assumed a simple Ekman drift for the ice trajectory.~~

~~The path of the ice, seen through its trajectory, appears to show a dependence of the choice of resolution in the vertical grid cell, but we cannot say for certain if it improves or deteriorates the results. ITP-52 has correlation coefficient of 0.87 on northward direction~~ and 0.82 ~~on eastward direction but due to accumulation of error both A0 and A1 fail to represent the actual trajectory of ITP-52 using just the start point and letting error accumulate through the entire ITP path that is 374 results in a pronounced difference in end points (Fig. 10).~~ correlation with speed magnitude. RMSE calculated for A1 based on Eq. (2) shows an error of 0.043 ms^{-1} and no significant bias.

3.~~1~~3 Temperature ~~and,~~ salinity, density and ~~Geopotential height~~MLD

~~3.3.1 Geopotential height~~

~~McPhee (2013) showed that the accumulation of freshwater in the Beaufort Gyre led to an increase in geopotential height and a strong geostrophic flow that may have feedbacks for the advection of ice out of the Canadian Arctic. Here, we~~

~~have used the model to calculate geopotential height (Fig. 12), referenced to the 400-m isobath and averaged from 2008-2011, with velocity vectors calculated based on the thermal wind equation. We can compare our result to hydrographic reports generated from ITPs and CTD cast during the same time period which has been reported in previous literature (McPhee 2013).~~

~~**Hydrographic data show a doming of about 45+ (cm) relative to geoid in Beaufort Gyre with the maximum centered at 74.5° N and 150° W (Kwok and Morison 2011, p. 20). Our model results show the same dome and correct sign, producing the correct geostrophic flow direction with the magnitude of 100+ (cm). The model shows the center of the dome to be around 80° N and 140W. Discrepancy between the magnitudes is in line with the results from sea-ice concentration section, with model over predicting the sea-ice extent hence generating excess fresh water. In a big picture this shows the capability of the model to predict the freshening of top 400 meter.**~~

3.3.1 Vertical Salinity and Temperature profiles

We chose 4 hydrographic profiles in the Beaufort ~~sea~~Sea to ~~represent~~assess the simulated vertical salinity and temperature. The first two sets of profiles are from ITP-1 winter ~~(Fig. 11)~~ and summer 2006 ~~(Fig. 11). The~~ ; the third set is from ITP-43 during winter 2010 ~~(Fig. 12)~~ and the fourth is from ITP-13 during summer 2008 (~~Fig. 13).~~Figure 5). For visualization we linearly extrapolated the profiles from the first layer of the model up to the surface, which overs the top 1 meter of the water column.

During winter time, the model T and S profiles show a well mixed layer ~~reaches~~that extends below 15 meters ~~in the model T and S profiles (Fig. 11),~~ followed by a very large gradient. The mixed-layer temperature is close to the local freezing point in a condition called “ice bath” (Shaw et al. 2009). The ITP profiles are similar; however the ITP mixed layer depth is deeper by nearly 10 meters, indicating more ice formation and convective heat loss over this water column, as compared to the model water column. In summer ~~(Fig. 11)~~ the model mixed layer shoals to approximately 5 meters depth following two local temperature extrema, the bigger maximum is at ~35 meters generated by intrusion of the Pacific Summer Water (PSW) which is a dominant feature in Canada basin. The second smaller maximum happens around 10 meters called Summer Mixed Layer (Shimada et al. 2001, p. 201) or Near-Surface Temperature Maximum (NSTM) (Jackson et al. 2010) which is a seasonal feature generated by shortwave solar heat diffusion (Donald K. Perovich 1990). These two well-defined phenomena are broadly descriptive of the summer surface layer in the Beaufort Gyre. They are; however, absent from the ITP data at this location, indicating a different ice and heat budget time history. ~~The mismatch in temperature is one of the challenges that numerical models face when reproducing the cold halocline. Recent studies show that eddies with diameter of approximately 30 km (Nguyen et al. 2012) have a major contribution in transport of PW from shelf break into Canadian basin, which requires a model with finer horizontal resolution.~~

Data and model profiles in ~~Fig. 12~~Figure 5b show better agreement in the shape and the absolute value of the T and S profiles. Both model and ITP data have a 20 meter deep mixed layer during 2010 winter. The model in this case does not show as much change in vertical temperature structure compared to actual data. In the profile from ITP-13 (~~Fig. 13~~Figure 5)

the model again over estimates the temperature beneath the mixed layer, although certain features including the NSTM can still be found near 10 meters, yet not as pronounced since it is very close to PSW. Bearing in mind that density in the Arctic is dominated by changes in salinity, we move forward to density profiles from this point on.

In addition, we note that recent studies show that eddies with diameters of 30 km or less (Nguyen et al. 2012; Spall et al. 2008; Zhao et al. 2014; Zhao and Timmermans 2015; Zhao et al. 2016) play an important role in transporting PW from the shelf break into Canadian basin. Adequate representation of ocean eddies and investigation their roles in setting the water column stratification require a model with finer horizontal resolution. Hence moving forward, in addition of A1, we utilize the 9km model (A2) to investigate the density profiles as well as study the MLD.

3.43.2 Density profiles

We ~~compare~~compared the ~~MITgcm~~36 km and 9 km model outputs of density to the time series of density profiles from ITP-~~62 (Fig. 15-16) during the course of nearly a year~~35 (Figure 6) starting in ~~Sep 2012.~~Oct 2009 to Mar 2010. A black mask indicates locations where there is no data from ITP-~~62~~35 - particularly in the upper 7 meters of the water column. As ITP-~~62~~35 transited through Canadian basin, density profiles ~~have~~contain both temporal and spatial changes ~~in them (Fig. 14).~~

We are able to discern some broad similarities ~~in~~between the model and ITP density profiles. From ~~September to mid-~~November~~, the density profile above 50 (m) tended to increase, consistent with the period of cooling and ice formation. From December~~ through ~~March~~January, both ITP and model density profiles remain relatively constant. Between February and March ~~and April~~, ITP-~~62~~35 appears to drift through a ~~unique water parcel, with lower~~zone of convection zone, likely caused by ice formation, with sudden increase of density ~~above 70 (m).~~near the surface. The same feature can be observed in ~~the MITgcm~~both A1 and A2 density. However, on a smaller scale, there is significantly more variation in the ITP data than what the model represents.

For exploring the reason behind the density signals ~~we are going to~~ use the simulated fraction of sea ice cover and ice thickness (~~Fig. 17~~Figure 6). The dominating effect appears to result from sea ice fraction ~~and~~ when there is almost continuously covered area. The changes from sea ice thickness can be observed in volume of fresh water in the water column~~. A peak~~, as seen by outcropping of the 1022.5 isopycnal coinciding with the increase of sea ice thickness. An increase in near surface density can be seen late in ~~March~~late January and early February accompanied by an increase in ice thickness and insertion of brine in the water column. The second peak, which is not as pronounced, happens in late February when ~~a decrease in~~ ice fraction decrease from 100% to ~~90%~~95% and exposed the surface water to cold atmosphere, ~~which generated~~leading to production of newly formed sea ice ~~and inserted brine into the water column. This signal will be~~. We further ~~discussed on mixed-layer~~examine these signals in MLD section~~.~~ below.

3.53.3 Mixed layer depth

There are many different methods in the literature for calculating mixed layer depth (Brainerd and Gregg 1995; Wijesekera and Gregg 1996; Thomson and Fine 2003; de Boyer Montégut et al. 2004; Lorbacher et al. 2006; Shaw et al. 2009). The

methods can be divided into two main types (Dong et al. 2008): The first type of algorithm looks for the depth (z_{MLD}) at which there has been a density increase of δρ between the ocean surface and z_{MLD}. A typical range of values for δρ are 0.005 (kg m^{-3}) to 0.125 (kg m^{-3}) (Brainerd and Gregg 1995; de Boyer Montégut et al. 2004). The second type uses slightly different criteria, where the base of the mixed layer is determined as the depth where the gradient of density ($\partial\rho/\partial z$) equals or exceeds a threshold; typical numbers for ($\partial\rho/\partial z$) are 0.005 (kg m^{-4}) to 0.05 (kg m^{-4}) (Brainerd and Gregg 1995; Lorbacher et al. 2006, p. 200). A more sophisticated approach to type 1 of ~~this~~these criteria is to utilize a differential between (ρ_{100m} - $\rho_{surface}$) as the cut of point (instead of using a fixed δρ) to account for the effects of surface ρ changes during winter and summer (Shaw et al. 2009). Here, we have implemented two of these methods M1 and M2, with M1 using δρ equal to 0.2 of ($\rho_{100m}-\rho_{surface}$) (Shaw et al. 2009) and M2 with a gradient ($\partial\rho/\partial z$) cut off point equal to 0.02 (kg m^{-4}) which matches innate model parametrization of MLD (Nguyen et al. 2009).

We compare these 2 methods by applying them to the profiles from ~~Fig. (10-11-12-13) which result~~Figure 5 and the results are shown in (~~Fig. 18~~Figure 7). In case (a) and (b) M1 produces a mixed layer depth that is 8 to 12 meters deeper, compared to the other method. A visual examination of profiles ~~appears to indicate~~indicates that the M1 criteria may be too flexible of a criteria. The results from ~~M2~~M1 appear to be intermittently "realistic", whereas ~~M1~~M2 can be difficult to implement ~~on~~data sampled at high vertical resolution ~~data with~~and contain greater small-scale variability. In practice, we find ~~M2~~M1 is the most straight-forward to implement.

It should be mentioned that it is difficult to consistently compare performance of the M1(δρ) and M2 methods on ITP and model data, because the model data extends to ~~the free surface, but~~top 1 m of water column, whereas the ITP data stops at 7 ~~(~~m~~)~~ depth (Peralta-Ferriz and Woodgate 2015). Furthermore, it has been shown that summer mixed layer in the Canada basin can be less than 12 meters (Toole et al. 2010). To account for this effect, we apply an additional restriction wherein any profile whose mixed-layer depth is less than 2 ~~(~~m~~)~~ below the shallowest ITP measurement is discarded. This restriction effectively removes any ML depths shallower than 10 meters due to ITP sampler not resolving the upper 8 ~~meters~~m of water column. In some cases, a remnant mixed-layer from the previous winter may exist in the water column. In this case, the methods incorrectly identify the remnant ML as actual ML depth.

To compare the methods over a longer time period, we calculated the mixed-layer depth from model data and ITP-~~62 data along the ITP-62 drift track. We used both M1 and M2 to determine the ML depth for the model data and for ITP-62 data (Fig. 19-20). M1 and M2 show almost similar results. The model shows a shallower ML compared to the ITP data; the most prominent feature in early March corresponds to a sudden change in density found in (Fig. 15). During the months of June and July, the model predicts zero mixed layers with stratification almost to the surface. The ITP data, beginning at 8 m cannot reflect this stratification, but we know this model result to be plausible based upon our comparisons with shipboard CTD profiles (data not shown here) and what is known about ice melting and stratification~~35 data along the ITP-35 drift track. We used M1 to determine the ML depth for A1, A2 and for ITP-35 data (Figure 8). Both model results show a shallower ML compared to the ITP data; the most prominent feature in late January corresponds to a sudden change in density found in (Figure 6). Beside the above mentioned peak A1 fails to capture any variability in MLD whereas A2 shows

that ML deepens by about 10 meters in mid February corresponding to ice opening occurring during the same time span (Figure 6). The difference between A1 and A2 and their ability to capture MLD change, can be explained by the capability of a higher resolution model to capture small-scale fractures in the ice cover (Figure 8), and conversely, the inability of the coarser resolution to do so is due to averaging over a larger grid. The wind appears to be the primary driving mechanism for the divergence in ice cover, which in turn exposes the ocean to the cold atmosphere and lead to a loss of buoyancy and an increase in MLD. With higher resolution these openings can be captured, leading to a better agreement with data in marginal ice zones. The changes in MLD are of first-order importance to the calculation of gas budgets such as the radon deficit. In this regard a fine-scale grid resolution has real advantages through its ability to capture both the ice advection and openings in ice cover that lead to MLD change. Coarser resolution would be justified when the point of interest is sufficiently far away from leads and marginal ice zones where the effect of sea-ice dynamics on MLD is important, so the effects of area averaging would be small enough to omit.

One last important note is the effect of the salt plume parameterization (SPP) on MLD. Nguyen et al. ~~For further exploring the forcing that drives the mixed layer, we use the Japanese reanalysis (JRA-25) (Onogi et al. 2007) wind speed, air temperature data and sea-ice fraction from the model and interpolated them on the path of ITP-62. The prominent feature during March to April can be explained by the reduction in ice cover to 95% , which resulted in water column exposure to low or moderate wind from 5 (ms^{-1}) to 10 (ms^{-1}) and low air temperatures, which in turn increased mixing and deepening of ML by 100% (Fig. 17). The wind appears to have led to a divergence in ice cover, which in-turn exposed the ocean to the cold atmosphere, leading to a loss of buoyancy and an increase in the mixed-layer depth. In this regard, the wind appears to play a facilitating role, leading to sea ice divergence, but there is no evidence to support that a strong wind event caused the mixed layer to deepen.~~

~~Further exploring the dependency of ML evolution to wind and temperature we calculated cross correlation between ML-wind and ML-temperature (Fig. 22). This analysis shows responses with respect to air temperature happen with no significant lag and wind with 10 days of delay which would result in a maximum 0.36 correlation for wind and 0.39 correlation for temperature. Without accounting for the effect of sea ice cover, which can somewhat modulate momentum inputs by the wind and strongly modulate heat and moisture fluxes, it appears that neither temperature nor wind has a dominant effect on MLD in the Arctic, but rather both play a role.~~

~~3.6 Circulation~~

~~The time-averaged upper ocean circulation in the Arctic has been described by oceanographers based upon the origin of the water masses that enter and exit the Arctic Ocean. These are primarily the Atlantic water (AW) and Pacific Water (PW). After entering the Arctic ocean AW and PW loose heat and sink, AW to between 200 (m) and 800 (m) (Golubeva and Platov 2007) and PW to between 50 and 150m (Steele et al. 2004). During the AOMIP intercomparison study it was observed that Arctic models can produce two AW circulation in opposing directions, with observations suggesting a cyclonic circulation in Arctic basins (Lindsay and Rothrock 1995). Potential vorticity influx from sub-Arctic oceans (Yang 2005) and unresolved~~

~~eddy parametrization (Holloway et al. 2007) have been shown to diminish this discrepancy and create consistent cyclonic circulation among all models (Proshutinsky et al. 2011).~~

~~We evaluated the capability of the model to reproduce the general circulation of Arctic by averaging output ocean velocities from A1 experiment during a time span of seven years from 2006 to 2012. We focused on two depth intervals 1-15 (m) depth to represent Ekman layer (Cole et al. 2014) (Fig. 24) and the second set is 180-250 m to model AW circulation (Fig. 23).~~

~~The flow field (Fig. 23) representing AW displays a counter-clockwise topographic boundary current in the Beaufort and Chukchi seas matching AW cyclonic circulation (Lindsay and Rothrock 1995; Proshutinsky et al. 2011). In contrast there is a clockwise boundary current in the southern Canadian basin (Fig. 24). These circulation patterns qualitatively match the hydrographic description of the time-mean circulation in the Arctic.~~

~~3.7~~(2009) demonstrated the need to remove the artificial excessive vertical mixing in coarse horizontal resolution models. To rule out the dependency of this parametrization to vertical resolution as a source in MLD bias, we preformed a suit of 1D tests, with and without the SPP on variety of vertical resolutions (not shown here) and sea ice melting/freezing scenarios and confirmed that SPP is not dependent on vertical grid spacing. We also investigated MLD in A3 (no SPP) run compared to A2, and confirmed the average MLD is the same between these 2 runs.

3.4 Velocities in the water column ~~beneath drifting sea ice~~

We have very little information from direct observations that permit us to track a water parcel especially beneath sea ice. This is one area where model output could be critical as there are not obvious alternatives. To ~~judge~~assess the consistency of the model water current field, we compared 2D model water velocity to data gathered from two sources: (1) from ADCPs mounted on moorings that were deployed starting in 2008 in Beaufort Gyre (Proshutinsky et al. 2009) and (2) the ITP-V sensor equipped with MAVS (Modular Acoustic Velocity Sensors) (Williams et al. 2010), which was the only operating ITP before 2013 which had an acoustic sensor mounted on it.

We compared the ~~magnitude of~~ velocity ~~without accounting~~components averaged from 5 m to 50 m to account for flow direction~~, i.e. removing~~ that is moving the ~~effects of Ekman turning (Cole et al. 2014)~~water parcels in ~~order to find a 2D-correlation~~the mixed layer over the duration of ITP-V working days which is from Oct 9, 2009 to Mar 31, 2010 (~~Fig. 25~~Figure 9). The ITP data has been daily averaged ~~so it matches the time interval of the model structure. Due to ITPs mechanical limitation on reporting velocities shallower than ~6 meters, the comparison starts from 7 meters.~~

~~The first result that emerges is that ITP velocity shows a lot more structure, changing speed at a much~~ to remove higher ~~time~~ frequency ~~most probably caused by eddies~~information which ~~has been shown to be a characteristic feature in the top layers of Beaufort Sea (Zhao et al. 2014). Figure 26-27 depicts the simulated and observed velocity components for ITP-V, to better compare the results the data and simulation have been filtered by 4 days low pass filter corresponding to 36 (km) in distance which the ITP travels effectively low pass filtering the results.~~we do not expect the model to capture due to the low frequency (6-hourly) wind forcing. Both A1 and A2 show less than 0.3 correlation with data with no improvement in respect to resolution.

~~The absolute 2D-correlation between the simulated and observed velocities for eastward direction is 20%, northward direction 22% and for the speed is 20%, these numbers represent r and not r2. We also compared the correlation versus depth and correlation of the velocity components and current speed (Fig. 28). If averaged over depth the northward velocities will have about 28% correlation with depth averaged data and also the correlation increases with depth after 40 meters. One possible reason for this lack of correlation near surface is effects of stratification in the model due to its shallower mixed layer.~~

~~Another source of ocean current data from the Arctic are ADCPs mounted on the moorings which has been deployed as part of Beaufort Gyre Observation System (BGOS), these profilers are located on the top float of subsurface moorings, measuring water velocities within the upper 30 meters of water column (Krishfield et al. 2014). Mooring D was the first mooring outfitted with an ADCP in 2005. Figure 29 shows the current speed measured by this mooring from October 2010, covering 1032 days of data located at 73.99° N and 139.98° W.~~

~~Simulation results follow certain features of the actual data (Fig. 29), high velocities around Jan-2011, Oct-2011 and Oct-2012 which is caused by exposure of water column surface to winds. In general, higher velocity magnitudes are observed which are not represented in the simulation.~~

~~For further exploring these high velocity features in the mooring data, we used wind speed from Japanese Reanalysis data (Onogi et al. 2007), sea-ice cover from satellite, constant sea-ice draft of 2m, sea-ice velocity estimation based on Sect. 3.2, Eq. (3) to construct a simple Ekman spiral based on Eq. (4) and Eq. (5). Our assumptions include a neutrally buoyant layer, constant dimensionless eddy viscosity (K* =0.2) (McPhee and Martinson 1992; McPhee 2012) and that our target depth is outside of the boundary (log) layer sea ice (Cole et al.~~ We further add A3 to our comparison for moorings velocities (Figure 9), and compared velocities at 25m, which is the level that is shared between all our models and removes the necessity of any interpolation. The simulation results show RMSE normalized by data of higher than 5 and correlations of less than 0.3 over 3 moorings and almost two years of data. This result indicates ocean currents are not well captured in the model irrespective of horizontal grid resolution. We must therefore look into the atmospheric forcing as a likely source of error on high frequency water velocities near surface. As noted above, the wind inputs into the model from the reanalyses are available at frequency 6-hourly. (Chaudhuri et al. 2014; Lindsay et al. 2014) have compared various available reanalysis products over the Arctic which we used to force our model, along with multiple other reanalysis products with available ship-based and weather station data and found out that wind products in all of those have low correlation i.e less than 0.2. To investigate we compared Jra55 and NCEP to a shipboard data gathered during 2014 in time span of 2 months in Arctic and found that JRA55 had -0.20 correlation, RMSE of 7.36 and bias of -1.3, NCEP had correlation of 0.10, RMSE of 5.73 and bias of -1.40 when compared with high frequency data on each cruise, reinforcing our suspicion of high frequency wind as a source of error in water currents.

4 Gas exchange estimation

Up to this point we have spent extensive effort assessing the skill of the MITgcm to reproduce the key forcing parameters listed in our introduction. This effort is motivated by the potential for using the MITgcm model output as a tool to improve our ability to model gas budgets in the IOBL and to improve our estimates of k in the sea ice zone, both of which depend on sea ice processes in the IOBL. To illustrate the potential impact that IOBL properties can have on the estimate of k, we perform a simple experiment, using estimates of k over the range of variation in model output at three locations in the sea ice zone. The intention is to illustrate the variability in k and in the radon deficit that can arise as a result of sea ice processes.

4.1 Constraining gas exchange forcings

Utilizing the results from section 3.1, 3.2 and 3.3, we calculated gas exchange velocities on P1, P2 and P3 (Figure 10), over the course of the model simulation (i.e. N = 7571) introduced in section 3.1. The MITgcm IOBL properties are fed to the estimator of k, considering sea ice processes (Loose et al. 2014). Our selected points has the SI concentrations of 96.1% , 87.62% and 61.69%, SI speeds of 0.05, 0.086 and 0.10 ms^{-1}, wind speed of 8.73, 5.87 and 4.11 ms^{-1}.

The result yields a point cloud of values that vary depending primarily on the range of ice velocity, wind speed and sea ice cover. The values of k range between 0.1 and 14.0, a mean of 2.4 and standard deviation of 1.55. This exercise demonstrates the sensitivity of k to the IOBL forcing parameters. In the event that we can trust the majority of the model outputs, such as the case here with high fidelity in the simulated SI concentration and SI velocities in A1, we conclude that, a numerical model, even a coarse resolution one, can make significant improvement to the estimate of k. The question of constraining the radon budget withing a Lagrangian water parcel is somewhat more complicated.

4.2 Application of forcings on Radon budget

The results in Section 3.4 showed that the difference between model and data water trajectories accumulated too much error to be useful (0.27), and indicate that for a regional GCM to be useful for reconstructing the back trajectories of radon-labeled water parcels, we will need improved wind-forcing fields. With current reanalysis products, finding the back trajectory of radon-labeled water parcel is not feasible. When improved wind fields are available, the Green's functions approach (Menemenlis et al. 2005; Nguyen et al. 2011) or adjoint method (Forget et al. 2015, p. 4; Wunsch and Heimbach 2013) can be used to reduce misfits between modeled and observed MLD velocity and likely make the model a valuable tool for tracking back trajectories, either in a smaller domain or full Arctic regional configuration. A possible source of wind data can be from shipboard measurements, assuming the measurements persist over 10 days in the given sampling station.

However, it may be possible to improve on the existing approach. When the drift trajectory is not known, one solution is to resort to averaging IOBL properties within a radius that is equal to the 30-day drift track (e.g. as done by Rutgers Van Der Loeff et al. 2014). The averages within this circle are treated as the representative IOBL properties. The radius of spatial averaging should be restricted by the average magnitude of the water parcel's velocity multiplied by the time span of interest.

When applying a spatial averaging, if the time scale of changes in forcings is smaller than time span of interest, the time dependency of forcings should be accounted for. Typically sea ice velocity is ~ 5 times greater than vertically averaged water velocity in mixed layer (Cole et al. 2014). In this regard, it may be acceptable to assume that the water parcel is stationary as long as ice advection is accounted for. Hence spatial averaging, should account for ice drift over the point of radon/radium sampling. The same logic also applies to the changes in the MLD and sea ice concentration. For example, gas exchange calculated (Eq. 1) based on assumption of constant MLD of 27.5 m with limits of 5 to 50 m (Peralta-Ferriz and Woodgate 2015), would have limits of ±80%, whereas gas exchange calculated based on model MLD would have ±50% error and accounts for time variability. With current level of uncertainty in reanalysis products, a mixed weighted combination of models outputs and shipboard data would be the way forward.

5. Summary

~~2014).~~

~~With z the distance from the water interface and $\boldsymbol{\tau}_{(z)}$ representing the shear vector, f Coriolis parameter and C_{ice} is the fraction of sea-ice cover. The interface friction velocity vector ($\mathbf{u}_{z_0}$) is calculated based on the type of interface. In case of water-ice interface $\mathbf{u}_{z_0}$ is based on law of the wall (McPhee 2008). Total Ekman velocity is C_{ice} weighted summation of Ekman vectors based on ice and air (Eq. 6), we then compared the velocity components based on this method, simulation and data (Fig. 30-31).~~

~~3.7.1 Sources of error in water column current velocities~~

~~There is 29% correlation between the simulation and mooring data. This is nearly identical to the poor correlation observed between the model and the ITP velocities. These discrepancies between model and data can be caused by several reasons. The first is the model resolution is too coarse to resolve mesoscale and submesoscale eddies, which have characteristic lengths of 10 km or smaller (Boccaletti et al. 2007; Timmermans et al. 2008). Because these eddies would all hypothetically fit within one of our 36-km grid boxes, this model configuration lacks the ability to represent them. Eddy resolving models have better agreement with velocity data (Holloway et al. 2011). Secondly the parameterization of sea-ice in the current model utilizes "levitating" sea-ice (Losch et al. 2010), meaning the sea-ice always stays on top of the free surface. This~~

assumption neglects the forcing caused by sea-ice advection whenever surface velocity is different than the sea-ice velocity (Campin et al. 2008). Neglecting the actual draft of sea-ice also introduces an error in calculating the correct distance from boundary which in turn makes the direction of velocity in Ekman spiral unreliable. Omission of other physics such as tidal waves, which is a common trait between arctic models, may as well have an effect on the velocity fields.

Having established that the correlation between the model output and mooring or ITP data is generally poor (i.e. 29% as reported above), we can further ask whether, in the absence of data, we would be just as well served by assuming that the current speeds are purely Ekman in nature. Using Eq. 4-6, as described above, we generated the Ekman spiral under partial ice cover to measure the current speed using only reanalysis winds. As with the model data, we compute the vertically-averaged current speed form 0 to 20 m depth. Using this assumption of Ekman drift and reanalysis winds, it is possible to reproduce the mooring velocity magnitude with 18% correlation. Whereas the 29% correlation between model and mooring data is unacceptable in most cases, it is still possible to argue that this is an improvement over the Ekman drift assumption. This is easily explained by the fact that the model captures more of the processes driving currents, including inertial oscillations.

In spite of the poor correlation between model and data, it captures many of the processes that drive net velocity, including Ekman, geostrophic, internal wave, inertial and subinertial processes. Consequently, we can use the model to determine the net drift and compare it to a typical geochemical assumption for Lagrangian drift. Here we refer to the approach employed by Rutgers Van Der Loeff et al. (2014). While evaluating radon deficits in the water column beneath variable ice cover, those authors assumed 0.5 cm/s bulk of mixed-layer speed and an elapsed time of 48 days to achieve a total drift of ~ 20 km. The 20 km becomes the radius over which ice cover is averaged to account for variations in surface area for exchange. We computed the 48 day back trajectory of water parcels originating from Mooring D for two years using simulated velocities and found out that the average distance between the start and end points is 10.3 Km, this number is 49% less that what was mentioned on previous literature (Rutgers Van Der Loeff et al. 2014). This difference is due to water parcel trajectory deviating from a straight line and having a circular motion between the start and end point.

4. Summary

We have used a 36-km version of , 9km and 2km versions of the ECCO ocean-sea ice coupled models based on the MITgcm to evaluateinvestigate whether coarse-resolutiona numerical model outputoutputs can be used to compensate for lack of data in constraining air-sea gas exchange rate in the Arctic. The goal wasis to understand if/how model outputs can improve estimation of gas exchange velocity calculation and to evaluate the capability of the model to use model output to interpret geochemical tracer fieldsfill in the missing information in radon deficiency method. This systematic comparison of upper ocean processes has revealed the following.

With regard to configuration, which was necessary to capture vertical profiles in near surface ocean, our experiments showed that changing the verticalThe coarse resolution of model grid cells reduced the accuracy of themodel showed a good fidelity in regard to reproducing sea- ice trajectory and concentration. This is likelyDepending on the location/season, the error of

simulated ice concentration varied between 0.02 and 0.2. Away from ice fronts or active melting/freezing zones the model tended to have higher accuracy. Even in the marginal ice zone, due to the ~~fact that the model output was tuned~~potentially high error in the satellite derived ice concentration, the model can still be used to quantify the air-sea gas exchange rate, though with ~~a different vertical grid spacing (Nguyen et al. 2011)~~an expected higher uncertainty due to the combination of model and ~~the tuning coefficients are no longer optimal, once~~data errors. In addition to sea ice concentration, we ~~change that spacing. It has been shown by (Holloway et al. 2011) that optimized parametrization of the model is sensitive to horizontal resolution; vertical resolution may as well have the same effect on the model.~~

~~We observed~~also found good correlation (~~78~~82%) between model ice ~~velocity~~speed and ITP drift. ~~The rapid accumulation of small errors in the drift speed and direction leads to significant differences in the predicted and actual drift trajectory. We found errors in drift trajectory of 2km/day. This relatively strong correlation is perhaps not surprising, considering that more than half of the ice drift variability can be explained by Ekman drift alone, and the model receives wind as an input parameter. It is also worth noting that by doubling the model resolution, error decreases by more than half, i.e. 0.8 (km/day) accuracy by using a 18-km model (Nguyen et al. 2011).~~

The estimation of mixed layer depth is challenging~~: No~~ due to its dependence on unconstrained density anomaly or density gradient thresholds. No MLD algorithm performs well in all situations~~;~~. In addition, CTD profiles from drifting buoys often do not include the top 7-10 m of the surface ocean where stratification can be important~~, and because the density structure~~. Adding to the challenge is the dependence of the ocean ~~is affected by~~ density structure on vertical fluxes ~~and by geostrophy.~~ In these model-data comparisons we found model MLD to be ~~biased~~ consistently ~~shallower, but this in part depends on a surface value, which is not recorded~~biased on the shallower side in all model resolution. We note however this result can partly be due to the missing upper 7m in moored drifters such as ITPs~~:~~ and thus resulting in a 1-sided bias in the observed MLD. The evolution of the ~~mixed layer~~mixing events showed that MLD correlates ~~equally well (or poorly if constrained by sea-ice) with wind and temperature trends (36% and 39% respectively). Despite the potential for bias in the model MLD, the time series of ITP and model MLD reveal that the model captures variability at a similar frequency. It appears 10-50% changes in MLD happen regularly over the course of days and major changes (i.e. 100-200 %) appear to be event-driven as opposed to gradual seasonal evolution.~~

~~The potential for such event-driven changes in the MLD in the time prior to sampling are clearly important to consider when evaluating surface ocean geochemical tracer fields, although it may be sufficient to look for large excursions in the wind, air temperature and~~to sea ice fraction: in areas of nearly full ice cover ~~from reanalysis data.~~

~~The A1 experiment showed a good visual representation of Arctic general circulation but on finer scales, individual flows did~~, small openings may result in exposure of water to the cold atmosphere and the resulting freezing events would deepen the mixed layer via brine rejection. The higher the resolution, the higher the capability of the model to capture these openings and the resulting deepening effects. The usage of the brine rejection scheme does not ~~match the data from ITPs or Mooring. This discrepancy may be the result of two causes - the lack of eddy resolving resolution and the lack of realistic ice physics. Holloway et al. (2011) have shown that by increasing the resolution to less than 9 (km) a good agreement can be~~

~~reached for 10 m vertical resolution. Our current lack of representation of velocity fields will lead to outcomes that are broadly similar, but locally incorrect. We further saw this effect on temperature profiles modeled on ITP path~~play an important role in determining the MLD.

~~We compare each of the variables affecting gas-exchange and summarize our comparison on Table-1. Overall, we find that a coarse-resolution model can yield as much as 50% improvement over simple assumptions that are loosely constrained by data (e.g. assuming Ekman drift or using a radius to average ice properties over a given time period). However, the coarse resolution model is not up to the task of representing Lagrangian drift of a water parcel. Water parcel drift beneath sea ice remains an elusive term, difficult to estimate, and hard to do without, when interpreting geochemical tracer fields.~~

The A1, A2 and A3 experiments consistently could not capture the water velocity observed in ITPs or Mooring. We speculate this discrepancy may be the result of the quality of the reanalysis wind product that is forcing these models. The wind product have been shown to have poor correlation with observed data at high frequencies. Considering that the response of near surface water is almost instantaneous to the wind forcing, low correlation in wind velocity would have direct impact on the modeled near surface water velocities and likely yield low correlations between modeled and observed ocean currents. On the other hand, the same wind field at lower frequencies and on broader spatial scale have higher accuracy, as evident by the high correlation between the modeled and observed sea ice velocity.

Taking into accounts all the misfits through detailed model-data comparisons, we were able to quantify the usefulness of a numerical model to improve gas exchange rate and parameterization methods. We showed an example on how the sea ice concentration, velocity and mixed-layer depth can affect gas-exchange rate by up to 200% in marginal sea ice zones and that the model outputs can help constrain this rate. By finding the low correlation in near surface ocean velocities, irrespective of model horizontal resolution, we concluded that finding the back trajectory of radon labeled water parcels is currently not feasible. Furthermore, we speculate the source for the common errors in our models, namely the low frequency and under-constrained atmospheric forcing fields, as well as identify alternative approaches to enable the use of a model to achieve the back trajectory calculation task. The alternative approach include using the MITgcm Green's functions and adjoint capability to help constrain the model ocean velocity to observations, and in a smaller dedicated domain based on the specific spatial distribution of data for both atmospheric winds and MLD ocean currents.

-

References

Acreman, D. M., and C. D. Jeffery, 2007: The use of Argo for validation and tuning of mixed layer models. *Ocean Model.*, **19**, 53–69, doi:10.1016/j.ocemod.2007.06.005.

Adcroft, A., and J.-M. Campin, 2004: Rescaled height coordinates for accurate representation of free-surface flows in ocean circulation models. *Ocean Model.*, **7**, 269–284, doi:10.1016/j.ocemod.2003.09.003.

Antonov, J., R. Locarnini, T. Boyer, A. Mishonov, and H. Garcia, World Ocean Atlas 2005 vol. 2 Salinity. *NOAA Atlas NESDIS*, **62**.

Bender, M. L., S. Kinter, N. Cassar, and R. Wanninkhof, 2011: Evaluating gas transfer velocity parameterizations using upper ocean radon distributions. *J. Geophys. Res.*, **116**, doi:10.1029/2009JC005805. http://doi.wiley.com/10.1029/2009JC005805 (Accessed April 20, 2014).

Blomquist, B. W., B. J. Huebert, C. W. Fairall, and I. C. Faloona, 2010: Determining the sea-air flux of dimethylsulfide by eddy correlation using mass spectrometry. *Atmospheric Meas. Tech.*, **3**, 1–20.

~~Boccaletti, G., R. Ferrari, and B. Fox-Kemper, 2007: Mixed Layer Instabilities and Restratification. *J. Phys. Oceanogr.*, **37**, 2228–2250, doi:10.1175/JPO3101.1.~~

de Boyer Montégut, C., G. Madec, A. S. Fischer, A. Lazar, and D. Iudicone, 2004: Mixed layer depth over the global ocean: An examination of profile data and a profile-based climatology. *J. Geophys. Res. Oceans*, **109**, C12003, doi:10.1029/2004JC002378.

Brainerd, K. E., and M. C. Gregg, 1995: Surface mixed and mixing layer depths. *Deep Sea Res. Part Oceanogr. Res. Pap.*, **42**, 1521–1543, doi:10.1016/0967-0637(95)00068-H.

Chaudhuri, A. H., R. M. Ponte, and A. T. Nguyen, 2014: A Comparison of Atmospheric Reanalysis Products for the Arctic Ocean and Implications for Uncertainties in Air–Sea Fluxes. *J.* ~~*Campin, J.-M., J. Marshall, and D. Ferreira, 2008: Sea ice–ocean coupling using a rescaled vertical coordinate z*. Ocean Model., **24**, 1–14, doi:10.1016/j.ocemod.2008.05.005.*~~

Clim., **27**, 5411–5421, doi:10.1175/JCLI-D-13-00424.1.

Cole, S. T., M.-L. Timmermans, J. M. Toole, R. A. Krishfield, and F. T. Thwaites, 2014: Ekman Veering, Internal Waves, and Turbulence Observed under Arctic Sea Ice. *J. Phys. Oceanogr.*, **44**, 1306–1328, doi:10.1175/JPO-D-12-0191.1.

Comiso, J., 2000: Bootstrap Sea Ice Concentrations from Nimbus-7 SMMR and DMSP SSM/I-SSMIS.

~~Comiso, J. C., 2008: *Bootstrap Sea Ice Concentrations from Nimbus-7 SMMR and DMSP SSM/I, 2004 to 2010*. National Snow and Ice Data Center, National Snow and Ice Data Center,.~~

Crabeck, O., B. Delille, S. Rysgaard, D. N. Thomas, N.-X. Geilfus, B. Else, and J.-L. Tison, 2014: First "in situ" determination of gas transport coefficients (DO2, DAr, and DN2) from bulk gas concentration measurements (O2, N2, Ar) in natural sea ice. *J. Geophys. Res. Oceans*, **119**, 6655–6668, doi:10.1002/2014JC009849.

Donald K. Perovich, G. A. M., 1990: Solar Heating of a Stratified Ocean in the Presence of a Static Ice Cover. *J. Geophys. Res.*, **95**, 18233–18245, doi:10.1029/JC095iC10p18233.

Dong, S., J. Sprintall, S. T. Gille, and L. Talley, 2008: Southern Ocean mixed-layer depth from Argo float profiles. *J. Geophys. Res. Oceans*, **113**, C06013, doi:10.1029/2006JC004051.

Fenty, I., and P. Heimbach, 2012: Coupled Sea Ice–Ocean-State Estimation in the Labrador Sea and Baffin Bay. *J. Phys. Oceanogr.*, **43**, 884–904, doi:10.1175/JPO-D-12-065.1.

Forget, G., J.-M. Campin, P. Heimbach, C. N. Hill, R. M. Ponte, and C. Wunsch, 2015: ECCO version 4: an integrated framework for non-linear inverse modeling and global ocean state estimation. *Geosci. Model Dev.*, **8**, 3071–3104, doi:10.5194/gmd-8-3071-2015.

Gerdes, R., and C. KöBerle, 2007: Comparison of Arctic sea ice thickness variability in IPCC Climate of the 20th Century experiments and in ocean-sea ice hindcasts. *J. Geophys. Res. Oceans*, **112**, C04S13, doi:10.1029/2006JC003616.

~~Golubeva, E. N., and G. A. Platov, 2007: On improving the simulation of Atlantic Water circulation in the Arctic Ocean. J. *Geophys. Res. Oceans*, **112**, C04S05, doi:10.1029/2006JC003734.~~

Heimbach, P., D. Menemenlis, M. Losch, J.-M. Campin, and C. Hill, 2010: On the formulation of sea-ice models. Part 2: Lessons from multi-year adjoint sea-ice export sensitivities through the Canadian Arctic Archipelago. *Ocean Model.*, **33**, 145–158, doi:10.1016/j.ocemod.2010.02.002.

H. J. Zemmelink, B. Delille, J. L. Tison, E. J. Hintsa, L. Houghton, and J. W.H. Dacey, 2006a: CO_2 deposition over multi-year ice of the western Weddell Sea. *Geophys. Res. Lett.*, **33**, doi:10.1029/2006GL026320.

H. J. Zemmelink, B. Delille, J. L. Tison, E. J. Hintsa, L. Houghton, and J. W.H. Dacey, 2006b~~W.H. Dacey, 2006~~: CO_2 deposition over multi-year ice of the western Weddell Sea. *Geophys. Res. Lett.*, **33**, doi:10.1029/2006GL026320.

Ho, D. T., C. S. Law, M. J. Smitth, P. Schlosser, M. Harvey, and P. Hill, 2006: Measurements of air-sea gas exchange at high wind speeds in the Southern Ocean: Implications for global parameterizations. *Geophys. Res. Lett.*, **33**, doi:10.1029/2006GL026817.

~~Holloway, G., and Coauthors, 2007: Water properties and circulation in Arctic Ocean models. *J.*~~ Ivanova, N., and Coauthors, 2015: Inter-comparison and evaluation of sea ice algorithms: towards further identification of challenges and optimal approach using passive microwave observations. *The Cryosphere*, **9**, 1797–1817, doi:10.5194/tc-9-1797-2015.

~~*Geophys. Res. Oceans*, **112**, C04S03, doi:10.1029/2006JC003642.~~

~~Holloway, G., A. Nguyen, and Z. Wang, 2011: Oceans and ocean models as seen by current meters. *J. Geophys. Res.*, **116**, doi:10.1029/2011JC007044. http://doi.wiley.com/10.1029/2011JC007044 (Accessed November 2, 2014).~~

Jackson, J. M., E. C. Carmack, F. A. McLaughlin, S. E. Allen, and R. G. Ingram, 2010: Identification, characterization, and change of the near-surface temperature maximum in the Canada Basin, 1993–2008. *J. Geophys. Res.*, **115**, doi:10.1029/2009JC005265. http://doi.wiley.com/10.1029/2009JC005265 (Accessed July 16, 2015).

Jähne, B., and H. Haubecker, 1998: Air-water gas exchange. *Annu. Rev. Fluid Mech.*, **30**, 443–448, doi:10.1146/annurev.fluid.30.1.443.

Johnson, M., S. Gaffigan, E. Hunke, and R. Gerdes, 2007: A comparison of Arctic Ocean sea ice concentration among the coordinated AOMIP model experiments. *J. Geophys. Res. Oceans*, **112**, C04S11, doi:10.1029/2006JC003690.

——, and Coauthors, 2012: Evaluation of Arctic sea ice thickness simulated by Arctic Ocean Model Intercomparison Project models. *J. Geophys. Res.*, **117**, doi:10.1029/2011JC007257. http://doi.wiley.com/10.1029/2011JC007257 (Accessed November 2, 2014).

Kara, A. B., 2003: Mixed layer depth variability over the global ocean. *J. Geophys. Res.*, **108**, doi:10.1029/2000JC000736. http://doi.wiley.com/10.1029/2000JC000736 (Accessed September 25, 2015).

Kohout, A. L., and M. H. Meylan, 2008: An elastic plate model for wave attenuation and ice floe breaking in the marginal ice zone. *J. Geophys. Res.*, **113**, doi:10.1029/2007JC004434.

Krishfield, R., J. Toole, A. Proshutinsky, and M.-L. Timmermans, 2008: Automated Ice-Tethered Profilers for Seawater Observations under Pack Ice in All Seasons. *J. Atmospheric Ocean. Technol.*, **25**, 2091–2105, doi:10.1175/2008JTECHO587.1.

Krishfield, R. A., A. Proshutinsky, K. Tateyama, W. J. Williams, E. C. Carmack, F. A. McLaughlin, and M.-L. Timmermans, 2014: Deterioration of perennial sea ice in the Beaufort Gyre from 2003 to 2012 and its impact on the oceanic freshwater cycle. *J. Geophys. Res. Oceans*, **119**, 1271–1305, doi:10.1002/2013JC008999.

~~Kwok, R., and J. Morison, 2011: Dynamic topography of the ice-covered Arctic Ocean from ICESat: DYNAMIC TOPOGRAPHY OF ARCTIC OCEAN. *Geophys. Res. Lett.*, **38**, n/a – n/a, doi:10.1029/2010GL046063.~~

Large, W. G., J. C. McWilliams, and S. C. Doney, 1994: Oceanic vertical mixing: A review and a model with a nonlocal boundary layer parameterization. *Rev. Geophys.*, **32**, 363–403, doi:10.1029/94RG01872.

Legge, O. J., D. C. E. Bakker, M. T. Johnson, M. P. Meredith, H. J. Venables, P. J. Brown, and G. A. Lee, 2015: The seasonal cycle of ocean-atmosphere CO2 flux in Ryder Bay, west Antarctic Peninsula. *Geophys. Res. Lett.*, **42**, 2015GL063796, doi:10.1002/2015GL063796.

Lindsay, R., M. Wensnahan, A. Schweiger, and J. Zhang, 2014: Evaluation of seven different atmospheric reanalysis products in the Arctic*. *J. Clim.*, **27**, 2588–2606.

Lindsay, R. W., and D. A. Rothrock, 1995: Arctic sea ice leads from advanced very high resolution radiometer images. *J. Geophys. Res.*, **100**, 4533–4544.

Locarnini, R., J. Mishonov, T. Boyer, J. I. Antonov, and H. E. Garcia, World Ocean Atlas 2005 vol. 1 Temreature. *NOAA Atlas NESDIS*, **62**.

Loose, B., W. R. McGillis, P. Schlosser, D. Perovich, and T. Takahashi, 2009: Effects of freezing, growth, and ice cover on gas transport processes in laboratory seawater experiments. *Geophys. Res. Lett.*, **36**, L05603, doi:10.1029/2008GL036318.

——, and Coauthors, 2011: Gas diffusion through columnar laboratory sea ice: implications for mixed-layer ventilation of CO2 in the seasonal ice zone. *Tellus B*, **63**, 23–39, doi:10.1111/j.1600-0889.2010.00506.x.

——, W. R. McGillis, D. Perovich, C. J. Zappa, and P. Schlosser, 2014: A parameter model of gas exchange for the seasonal sea ice zone. *Ocean Sci.*, **10**, 1–16, doi:10.5194/os-10-1-2014.

Loose, B., R. Kelly, A. Bigdeli, R. . Krishfield, M. Rutgers Van Der Loeff, and B. Moran, 2016: How well does wind speed predict air-sea gas transfer in the sea ice zone? A synthesis of radon deficit profiles in the upper water column of the Arctic Ocean. *J. Geophys. Res.*,.

Lorbacher, K., D. Dommenget, P. P. Niiler, and A. Köhl, 2006: Ocean mixed layer depth: A subsurface proxy of ocean-atmosphere variability. *J. Geophys. Res. Oceans*, **111**, C07010, doi:10.1029/2003JC002157.

Losch, M., D. Menemenlis, J.-M. Campin, P. Heimbach, and C. Hill, 2010: On the formulation of sea-ice models. Part 1: Effects of different solver implementations and parameterizations. *Ocean Model.*, **33**, 129–144, doi:10.1016/j.ocemod.2009.12.008.

Marshall, J., A. Adcroft, C. Hill, L. Perelman, and C. Heisey, 1997: A finite-volume, incompressible Navier Stokes model for studies of the ocean on parallel computers. *J. Geophys. Res. Oceans*, **102**, 5753–5766, doi:10.1029/96JC02775.

McPhee, M., and D. G. Martinson, 1992: Turbulent mixing under drifting pack ice in the Weddell Sea. *Science*, **263**, 218–220.

McPhee, M. G., 2008: *Air-ice-ocean interaction: Turbulent ocean boundary layer exchange*. Springer, New York,.

McPhee, M. G., 2012: Advances in understanding ice–ocean stress during and since AIDJEX. *Cold Reg. Sci. Technol.*, **76-77**, 24–36, doi:10.1016/j.coldregions.2011.05.001.

——, 2013: Intensification of Geostrophic Currents in the Canada Basin, Arctic Ocean. *J. Clim.*, **26**, 3130–3138, doi:10.1175/JCLI-D-12-00289.1.

McPhee, M. G., A. Proshutinsky, J. H. Morison, M. Steele, and M. B. Alkire, 2009: Rapid change in freshwater content of the Arctic Ocean. *Geophys. Res. Lett.*, **36**, L04606, doi:10.1029/2008GL036587.

Menemenlis, D., I. Fukumori, and T. Lee, 2005: Using Green's Functions to Calibrate an Ocean General Circulation Model. *Mon. Weather Rev.*, **133**, 1224–1240, doi:10.1175/MWR2912.1.

——, J.-M. Campin, P. Heimbach, C. Hill, T. Lee, A. Nguyen, M. Schodlok, and H. Zhang, 2008: ECCO2: High resolution global ocean and sea ice data synthesis. *Mercat. Ocean Q. Newsl.*, **31**, 13–21.

Morison, J. H., M. McPhee, T. B. Curtin, and T. B. Paulson, 1992: The oceanography of winter leads. *J. Geophys. Res.*, **97**, 11199–11218.

Nguyen, A. T., D. Menemenlis, and R. Kwok, 2009: Improved modeling of the Arctic halocline with a subgrid-scale brine rejection parameterization. *J. Geophys. Res.*, **114**, doi:10.1029/2008JC005121. http://doi.wiley.com/10.1029/2008JC005121 (Accessed November 2, 2014).

Nguyen, A. T., D. Menemenlis, and R. Kwok, 2011: Arctic ice-ocean simulation with optimized model parameters: Approach and assessment. *J. Geophys. Res. Oceans*, **116**, C04025, doi:10.1029/2010JC006573.

——, R. Kwok, and D. Menemenlis, 2012: Source and Pathway of the Western Arctic Upper Halocline in a Data-Constrained Coupled Ocean and Sea Ice Model. *J. Phys. Oceanogr.*, **42**, 802–823, doi:10.1175/JPO-D-11-040.1.

Nightingale, P. D., ~~P. S. Liss, and P. Schlosser, 2000: Measurements of air-sea gas transfer during an open ocean algal bloom. *Geophys. Res. Lett.*, **27**, 2117–2120~~G. M. Malin, C. Law, A. Watson, P. S. Liss, M. I. Liddicoat, J. Boutin, and R. C. Upstill-Goddard, 2000a: In situ evaluation of air-sea gas exchange parameterizations using novel conservative and volatile tracers. *Glob. Biogeochem. Cycles*, **14**, 373–387.

——, ——, ——, ——, ——, ——, ——, and ——, 2000b: In situ evaluation of air-sea gas exchange parameterizations using novel conservative and volatile tracers. *Glob. Biogeochem. Cycles*, **14**, 373–387.

Ohno, Y., N. Iwasaka, F. Kobashi, and Y. Sato, 2008: Mixed layer depth climatology of the North Pacific based on Argo observations. *J. Oceanogr.*, **65**, 1–16, doi:10.1007/s10872-009-0001-4.

Onogi, K., and Coauthors, 2007: The JRA-25 Reanalysis. *J. Meteorol. Soc. Jpn. Ser II*, **85**, 369–432, doi:10.2151/jmsj.85.369.

~~Park, H.-S., and A. L. Stewart, 2015: An analytical model for wind-driven Arctic summer sea ice drift. *Cryosphere Discuss.*, **9**, 2101–2133, doi:10.5194/tcd-9-2101-2015.~~

Peng, T.-H., W. S. Broecker, G. G. Mathieu, and Y.-H. Li, 1979: Radon evasion rates in the Atlantic and Pacific oceans as determined during the Geosecs program. *J. Geophys. Res.*, **84**, 2471–2486.

Peralta-Ferriz, C., and R. A. Woodgate, 2015: Seasonal and interannual variability of pan-Arctic surface mixed layer properties from 1979 to 2012 from hydrographic data, and the dominance of stratification for multiyear mixed layer depth shoaling. *Prog. Oceanogr.*, **134**, 19–53, doi:10.1016/j.pocean.2014.12.005.

Proshutinsky, A., and Coauthors, 2001: Multinational effort studies differences among arctic ocean models. *Eos Trans. Am. Geophys. Union*, **82**, 637–644, doi:10.1029/01EO00365.

Proshutinsky, A., R. Gerdes, D. Holland, G. Holloway, and M. Steele, 2008: AOMIP: coordinated activities to improve models and model predictions. *CLIVAR Exch. 131 Exch. 44*, **17**. http://eprints.soton.ac.uk/50120/01/Exch_44.pdf (Accessed September 5, 2015).

Proshutinsky, A., and Coauthors, 2009: Beaufort Gyre freshwater reservoir: State and variability from observations. *J. Geophys. Res.*, **114**, doi:10.1029/2008JC005104. http://doi.wiley.com/10.1029/2008JC005104 (Accessed June 15, 2015).

Proshutinsky, A., and Coauthors, 2011: Recent advances in Arctic ocean studies employing models from the Arctic Ocean Model Intercomparison Project. *Oceanography*, **24**, 102–113, doi:10.5670/oceanog.2011.61.

Rutgers Van Der Loeff, M., N. Cassar, M. Nicolaus, B. Rabe, and I. Stimac, 2014: The influence of sea ice cover on air-sea gas exchange estimated with radon-222 profiles. *J. Geophys. Res. - Oceans*, **119**, 2735–2751, doi:10.1002/2013JC009321.

Salter, M. E., and Coauthors, 2011: Impact of an artificial surfactant release on air-sea gas fluxes during Deep Ocean Gas Exchange Experiment II. *J. Geophys. Res.*, **116**, C11016, doi:10.1029/2011JC007023.

Shaw, W. J., T. P. Stanton, M. G. McPhee, J. H. Morison, and D. G. Martinson, 2009: Role of the upper ocean in the energy budget of Arctic sea ice during SHEBA. *J. Geophys. Res.*, **114**, doi:10.1029/2008JC004991. http://doi.wiley.com/10.1029/2008JC004991 (Accessed July 15, 2015).

Shimada, K., E. C. Carmack, K. Hatakeyama, and T. Takizawa, 2001: Varieties of shallow temperature maximum waters in the western Canadian Basin of the Arctic Ocean. *Geophys. Res. Lett.*, **28**, 3441–3444.

Smethie, W. M., T. Takahashi, D. W. Chipman, and J. R. Ledwell, 1985: Gas Exchangeandexchange and CO2 Fluxflux in the Tropicaltropical Atlantic Ocean Determineddetermined from 222Rn and pCO2 measurements. *J. Geophys. Res.*, *Oceans 1978–2012*, **90**, 7005–7022.

SteeleSpall, M., J. Morison, W. Ermold, I. Rigor, A., R. S. Pickart, P. S. Fratantoni M. Ortmeyer, and K. Shimada, 2004: Circulation of summer Pacific halocline water in theA. J. Plueddemann, 2008: Western Arctic Ocean.Shelfbreak Eddies: Formation and Transport. *J. Geophys. Res. Oceans*, ***109***, *C02027Phys. Oceanogr.*, **38**, 1644–1668, doi:10.1029/2003JC002009175/2007JPO3829.1.

Sweeney, C., E. Gloor, A. R. Jacobson, R. M. Key, G. McKinley, J.-L. Sarmiento, and R. Wanninkhof, 2007: Constraining global air-sea gas exchange for CO2 with recent bomb 14C measurements. *Glob. Biogeochem. Cycles*, **21**, doi:10.1029/2006GB002784.

Takahashi, T., and Coauthors, 2009: Climatological Mean and Decadal Change in Surface Ocean pCO_2, and Net Sea-air CO_2 Flux over the Global Oceans. *Deep-Sea Res. Part II*, **56**, 554–577.

Thomson, R. E., and I. V. Fine, 2003: Estimating Mixed Layer Depth from Oceanic Profile Data. *J. Atmospheric Ocean. Technol.*, **20**, 319–329, doi:10.1175/1520-0426(2003)020<0319:EMLDFO>2.0.CO;2.

Timmermans, M.-L., J. Toole, A. Proshutinsky, R. Krishfield, and A. Plueddemann, 2008: Eddies in the Canada Basin, Arctic Ocean, Observed from Ice-Tethered Profilers. *J. Phys. Oceanogr.*, **38**, doi:10.1175/2007JPO3782.1.

———, A. Proshutinsky, R. A. Krishfield, D. K. Perovich, J. A. Richter-Menge, T. P. Stanton, and J. M. Toole, 2011: Surface freshening in the Arctic Ocean's Eurasian Basin: An apparent consequence of recent change in the wind-driven circulation. *J. Geophys. Res.*, **116**, doi:10.1029/2011JC006975. http://doi.wiley.com/10.1029/2011JC006975 (Accessed November 2, 2014).

Toole, J. M., M.-, L. Timmermans, D. K. Perovich, R. A. Krishfield, A. Proshutinsky, and J. A. Richter-Menge, 2010: Influencesnfluences of the ocean surface mixed layer and thermohaline stratification on Arctic Sea ice in the central Canada Basin. *J. Geophys. Res.*, **115**, doi:10.1029/2009JC005660. http://doi.wiley.com/10.1029/2009JC005660 (Accessed June 15, 2015).

Wadhams, P., V. A. Squire, J. A. Ewing, and R. W. Pascal, 1986: The effect of the marginal ice zone on the directional wave spectrum of the ocean. *J. Phys. Oceanogr.*, **16**, 358–376.

Wanninkhof, R., 1992: Relationship between wind speed and gas exchange over the ocean. *J. Geophys. Res. Oceans*, **97**, 7373–7382, doi:10.1029/92JC00188.

Wanninkhof, R., and W. R. McGillis, 1999: A cubic relationship between air-sea CO2 exchangeand wind speed. *Geophys. Res. Lett.*, **26**, 1889–1892.

Wijesekera, H. W., and M. C. Gregg, 1996: Surface layer response to weak winds, westerly bursts, and rain squalls in the western Pacific warm pool. *J. Geophys. Res. Oceans*, **101**, 977–997, doi:10.1029/95JC02553.

Williams, A. J., F. T. Thwaites, A. T. Morrison, J. M. Toole, and R. A. Krishfield, 2010: Motion tracking in an acoustic point-measurement current meter. OCEANS 2010, IEEE.

Yang, J., 2005: The Arctic and Subarctic Ocean Flux of Potential Vorticity and the Arctic Ocean Circulation*. *J. Phys. Oceanogr.*, **35**, 2387–2407, doi:10.1175/JPO2819.1.

Wunsch, C., and P. Heimbach, 2013: Dynamically and Kinematically Consistent Global Ocean Circulation and Ice State Estimates. *In Ocean Circulation and Climate: A 21 Century Perspective*, Elsevier BV https://dash.harvard.edu/handle/1/12136112 (Accessed November 30, 2016).

Zemmelink, H. J., J. W. H. Dacey, L. Houghton, E. J. Hintsa, and P. S. Liss, 2008: Dimethylsulfide emissions over the multi-year ice of the western Weddell Sea. *Geophys. Res. Lett.*, **35**, doi:10.1029/2007GL031847.

Zhang, J., and D. A. Rothrock, 2003: Modeling Global Sea Ice with a Thickness and Enthalpy Distribution Model in Generalized Curvilinear Coordinates. *Mon. Weather Rev.*, **131**, 845–861, doi:10.1175/1520-0493(2003)131<0845:MGSIWA>2.0.CO;2.

Zhao, M., and M.-L. Timmermans, 2015: Vertical scales and dynamics of eddies in the Arctic Ocean's Canada Basin. *J. Geophys. Res.M.-L. Timmermans, S. Oceans*, **120**, 8195–8209, doi:10.1002/2015JC011251.

———, ———, S. Cole, R. Krishfield, A. Proshutinsky, and J. Toole, 2014: Characterizing the eddy field in the Arctic Ocean halocline. *J. Geophys. Res. Oceans*, **119**, 8800–8817, doi:10.1002/2014JC010488.

———, ———, ———, ———, and J. Toole, 2016: Evolution of the eddy field in the Arctic Ocean's Canada Basin, 2005–2015. *Geophys. Res.*

Figures

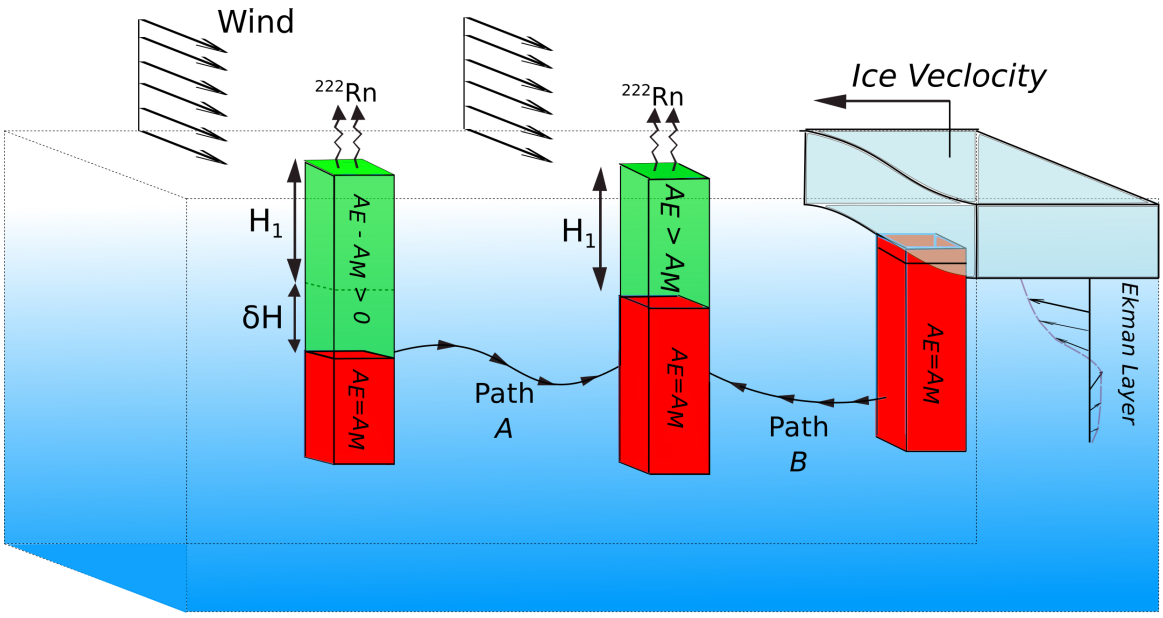

Fig 1. A graphic illustration of two possible back trajectory of a single sampling station

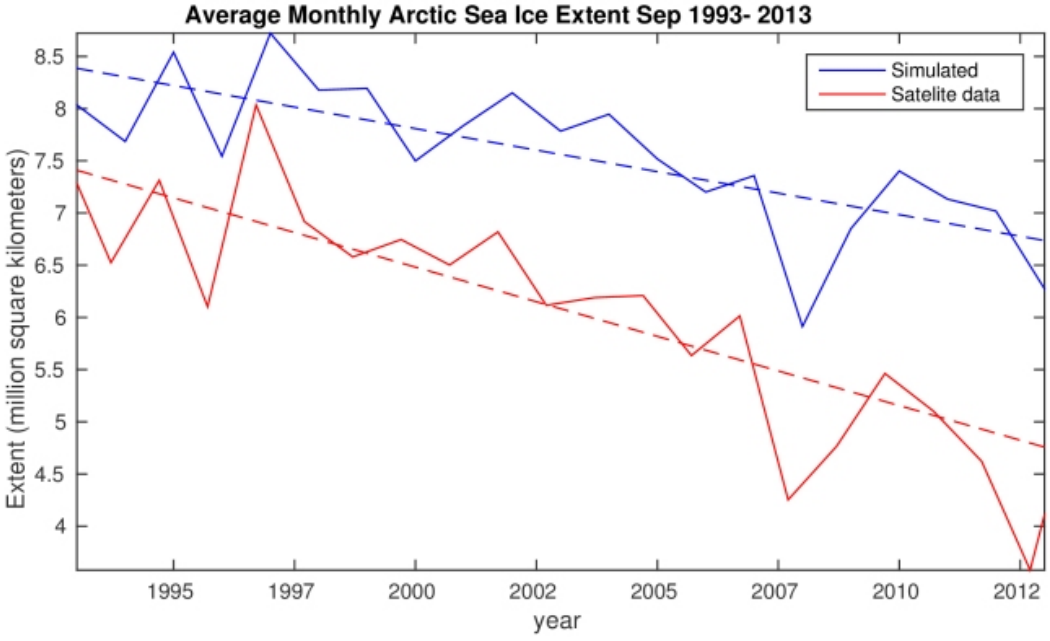

Fig 2. Arctic Sea-ice extent from 1992-2012 using A0

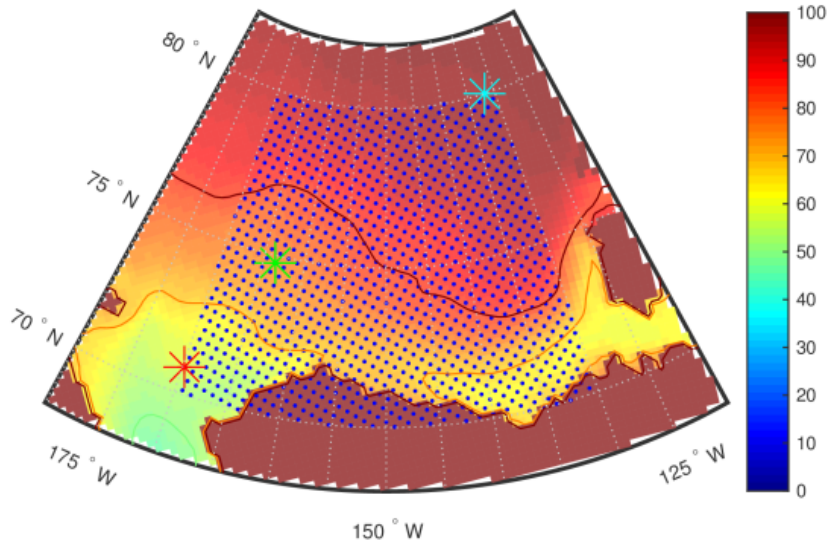

Fig 3. Averaged satellite sea ice cover from 2006-2013, Solid red line marking 80% cover and orange line marking 60%, Blue dots show the analysis grid, stars show the location of the three points Cyan P1, Green P2, Red P3 where time series data is graphed in Figure 3.

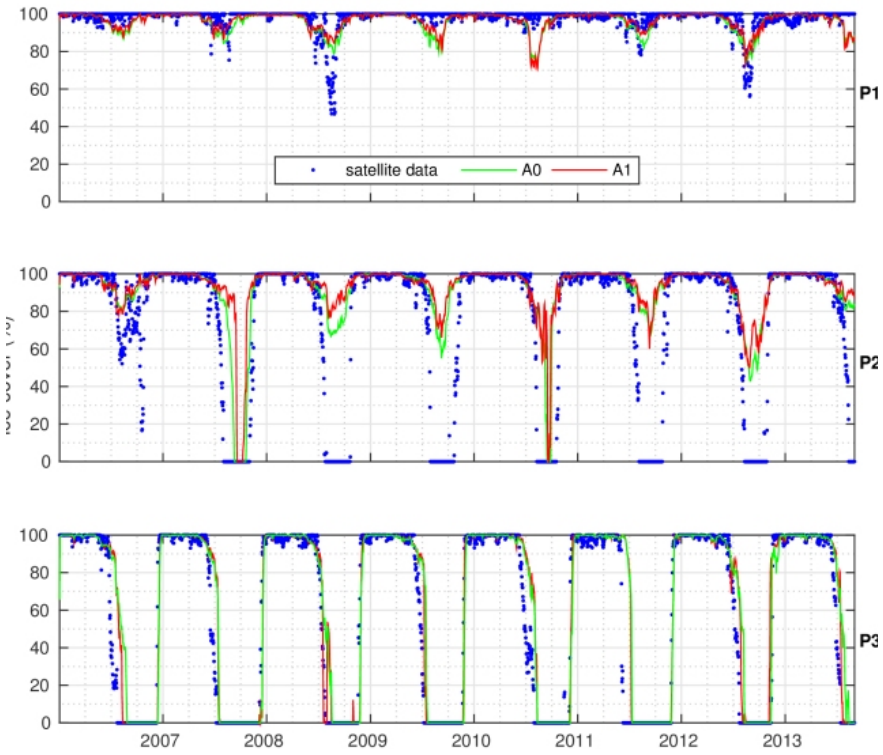

Fig 4. Time history of Sea-Ice fraction from top P1, P2 and P3, Satellite data compared with model results A0 and A1

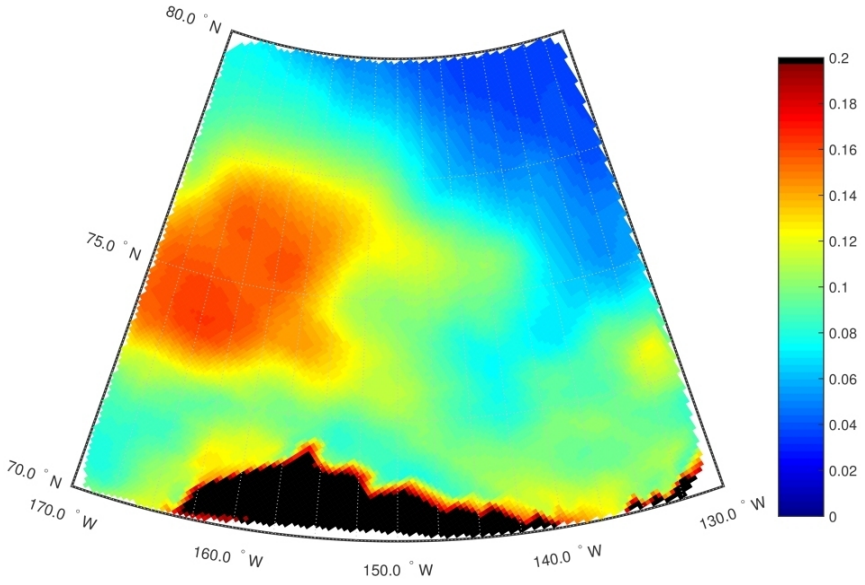

~~Fig 5. Root mean square error averaged of A1 over time from 2006 to 2013; black mask covers the grid points on the ground~~

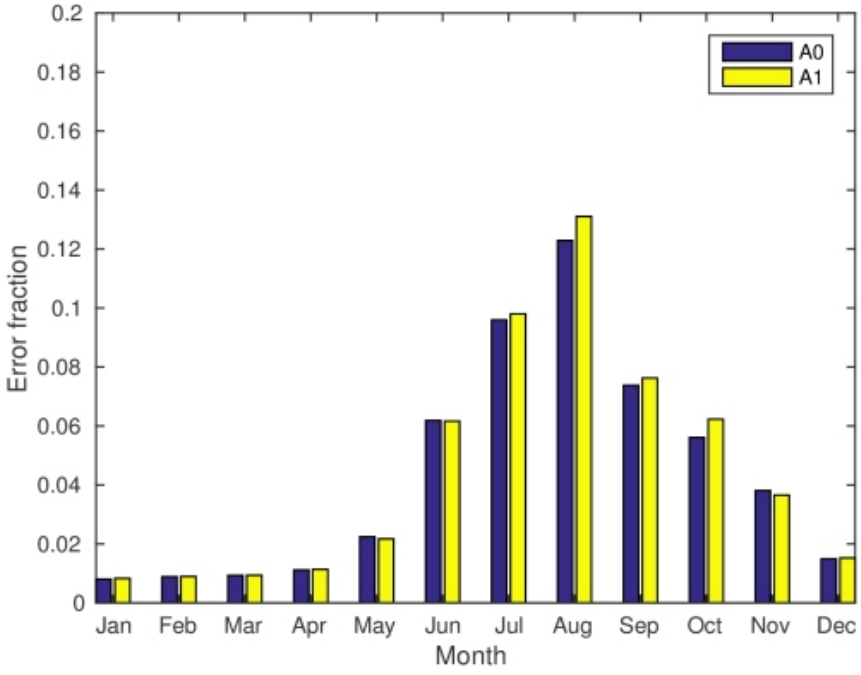

Fig 6. Monthly averaged Annual Root Mean Square Error

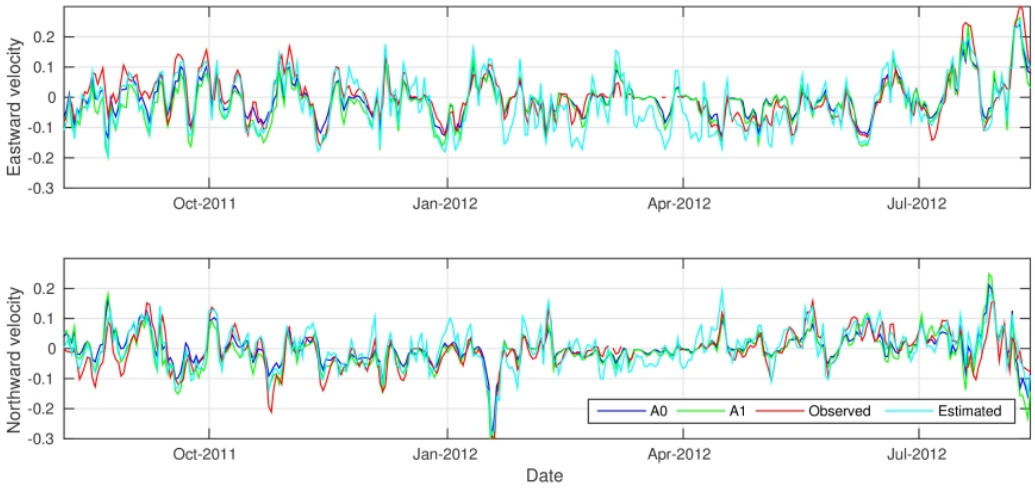

Fig 7. Velocity components from A0 and A1 compared with drift velocity of ITP-53

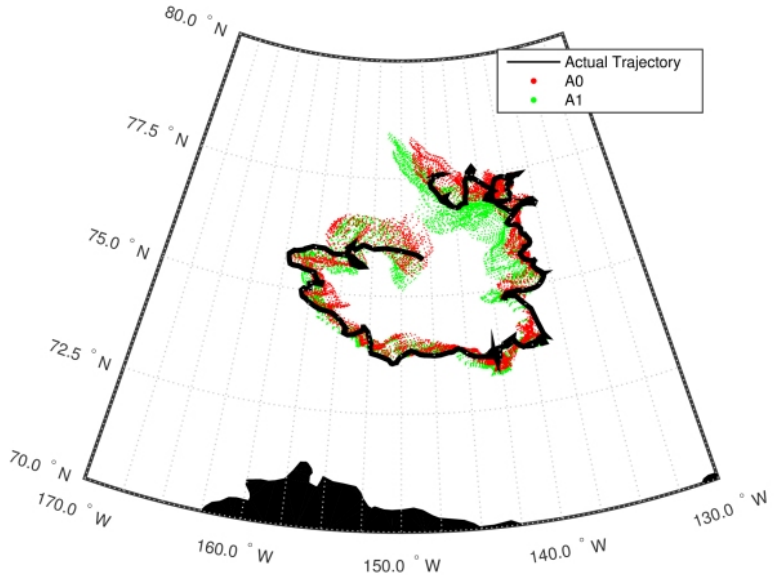

Fig 8. 30 day trajectory of ITP 53, starting August 2011 to August 2012

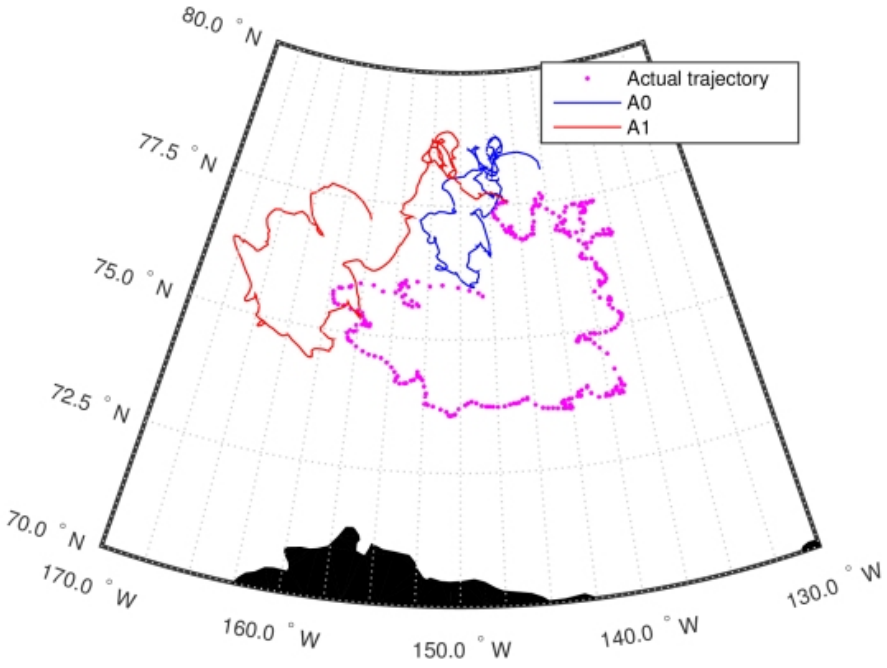

Fig 9. Simulated and observed trajectory of ITP53, Aug 06 2011 to Aug 13 2012

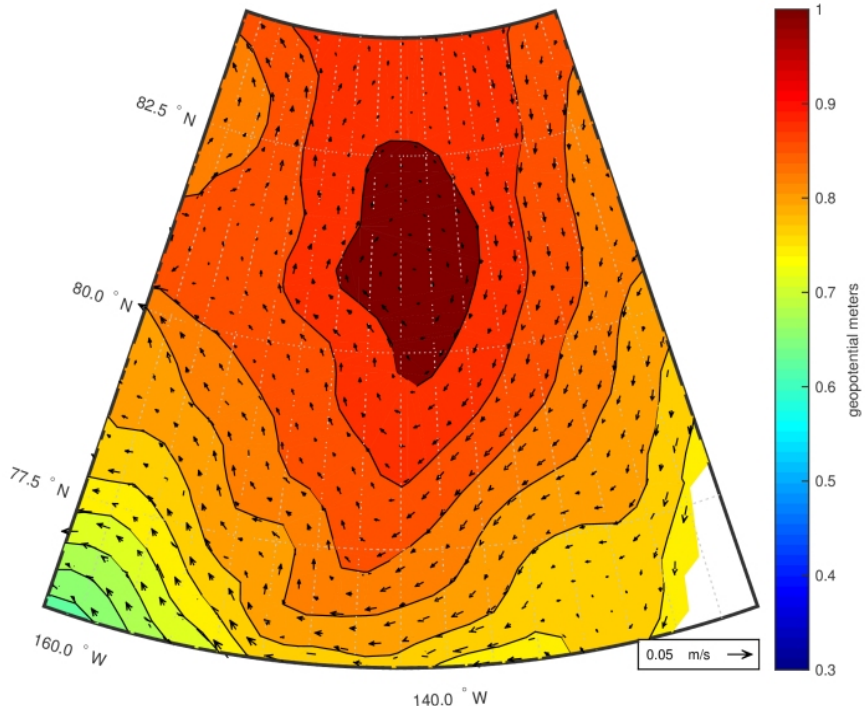

Fig 10. MITgcm geopotential height referenced to 400(m), 2008-2011

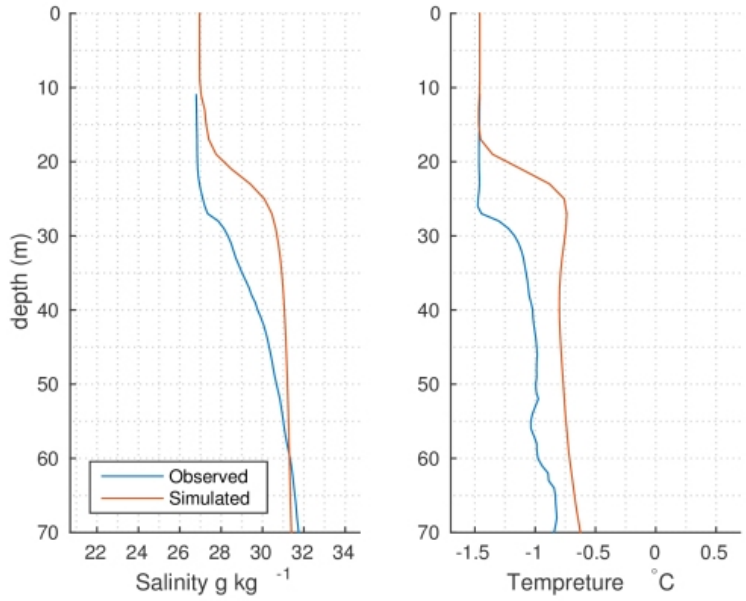

Fig 11. Obtained from ITP 1 on 13-Dec-2006 at 74.80°N and 131.44°W

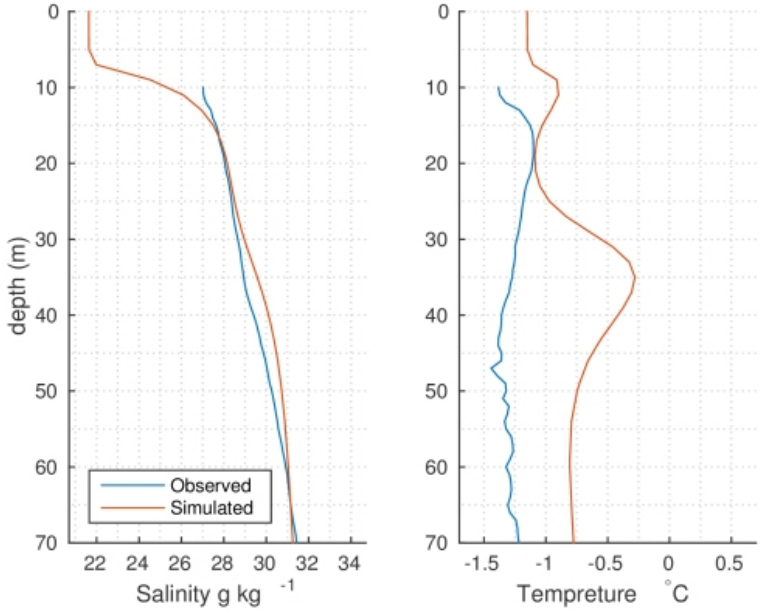

Fig 12: Obtained from ITP 1 on 28-Aug-2006 at 76.96°N and 133.32°W

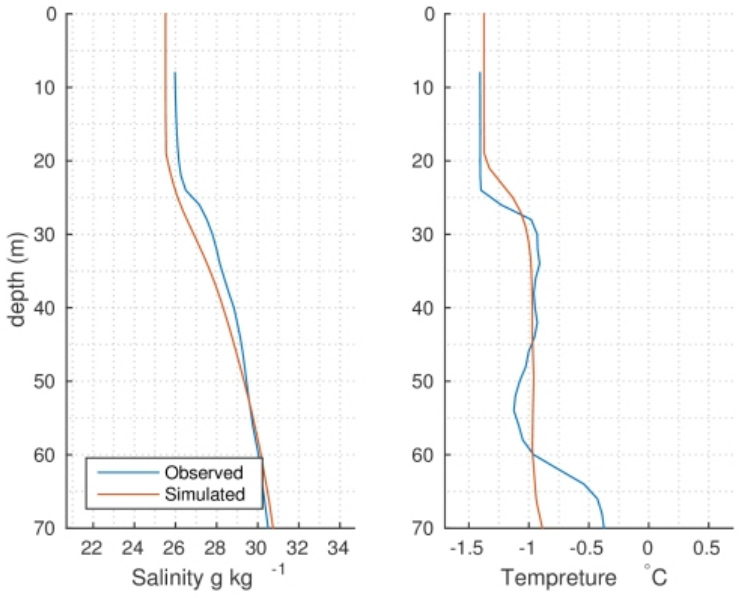

Fig 13. Obtained from ITP-43 on 27-Nov-2010 at 75.41°N and 143.09°W

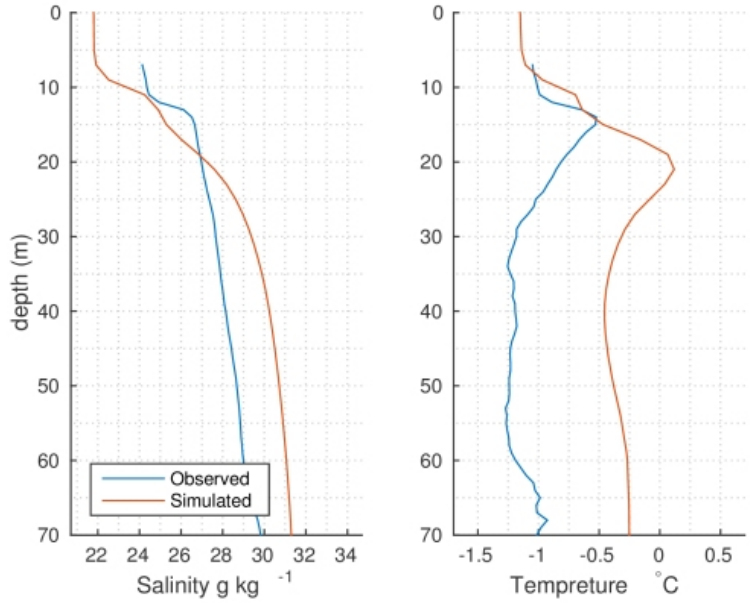

Fig 14: Obtained from ITP-13 on 30-Jul-2008 at 75.00°N and 132.78°W

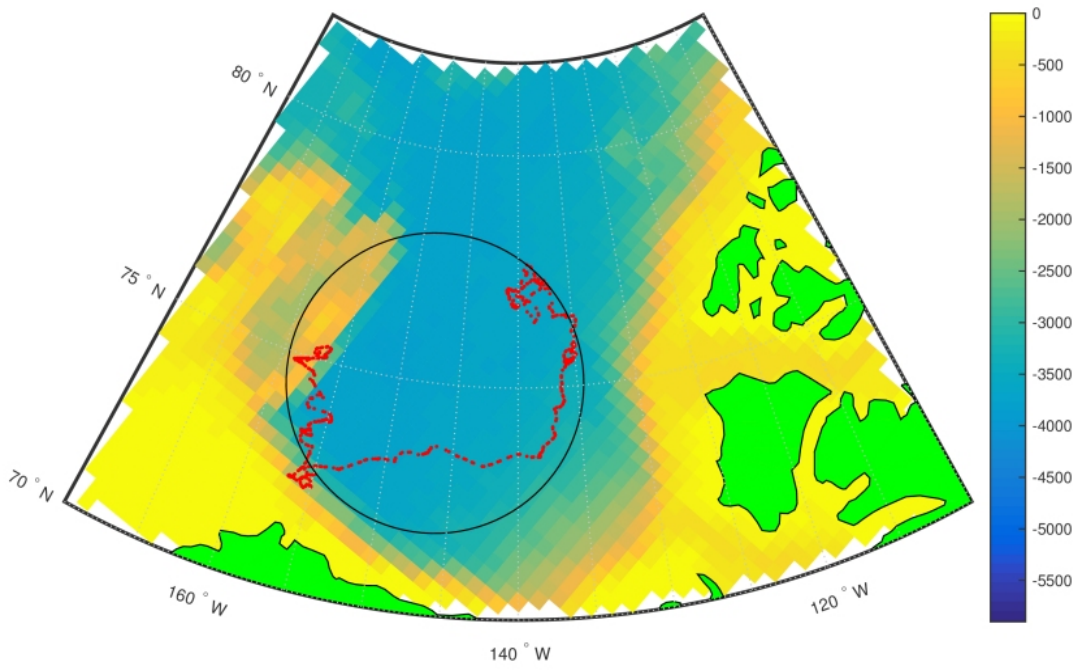

Fig 15. ITP-62 distribution of sampling stations and the circle centered at 75N 147 W and radius of 330 (km)

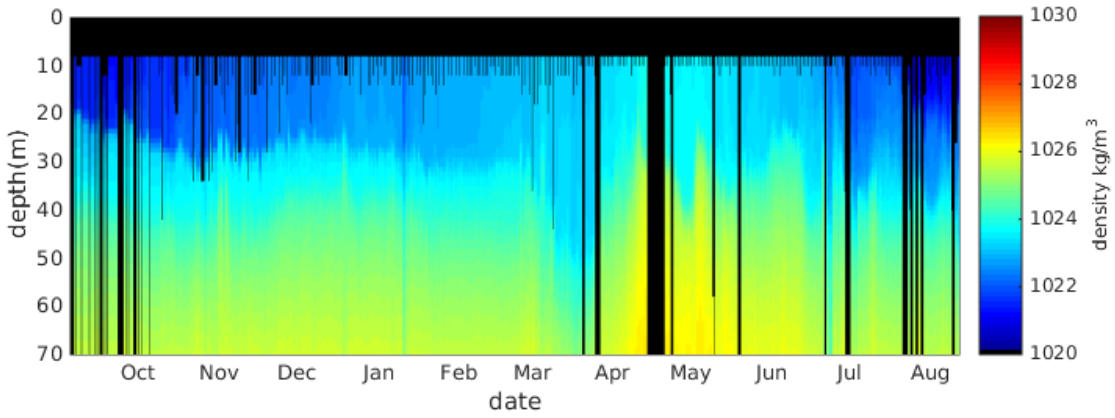

Fig 16. Observed upper ocean density, ITP 62 Sep 04 2012 to 12 Aug 2013

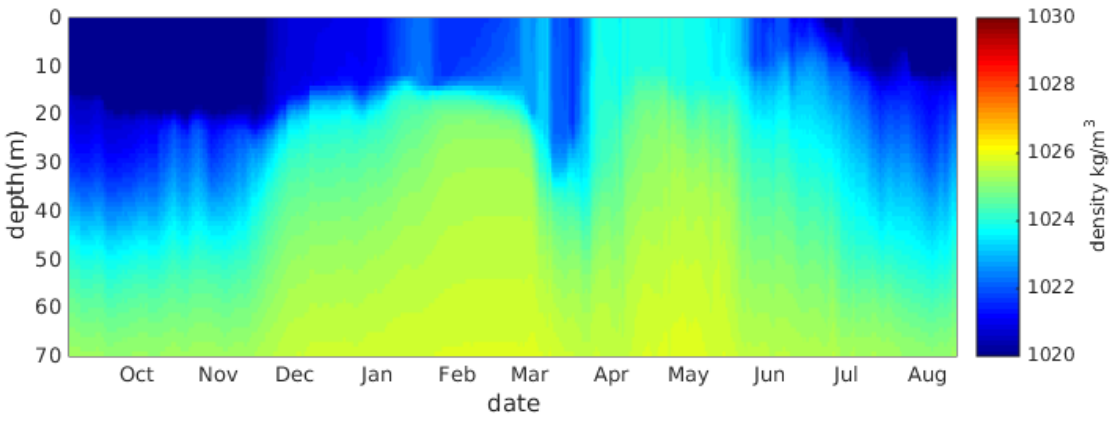

Fig 17. Simulated upper ocean density following ITP-62

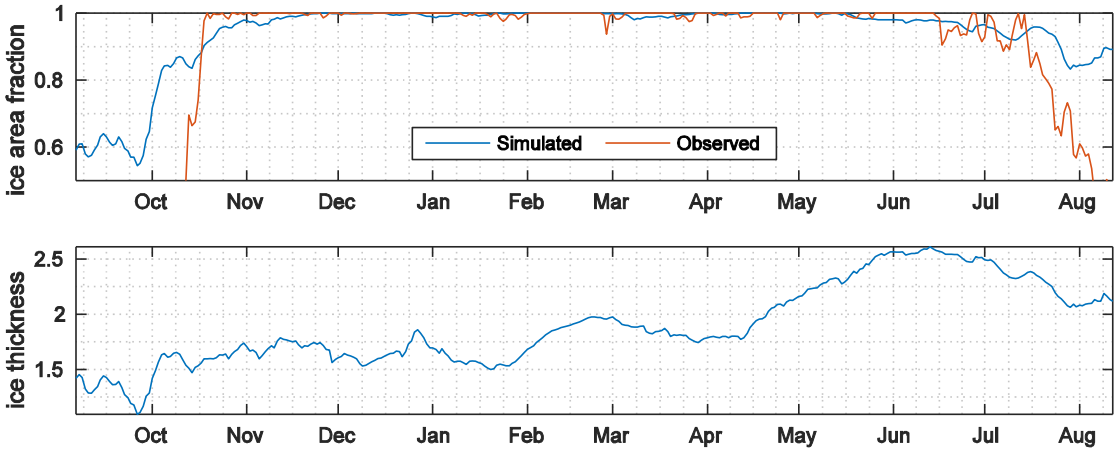

Fig. 18: Sea Ice fraction and Modeled Ice thickness interpolated into ITP-62 drift

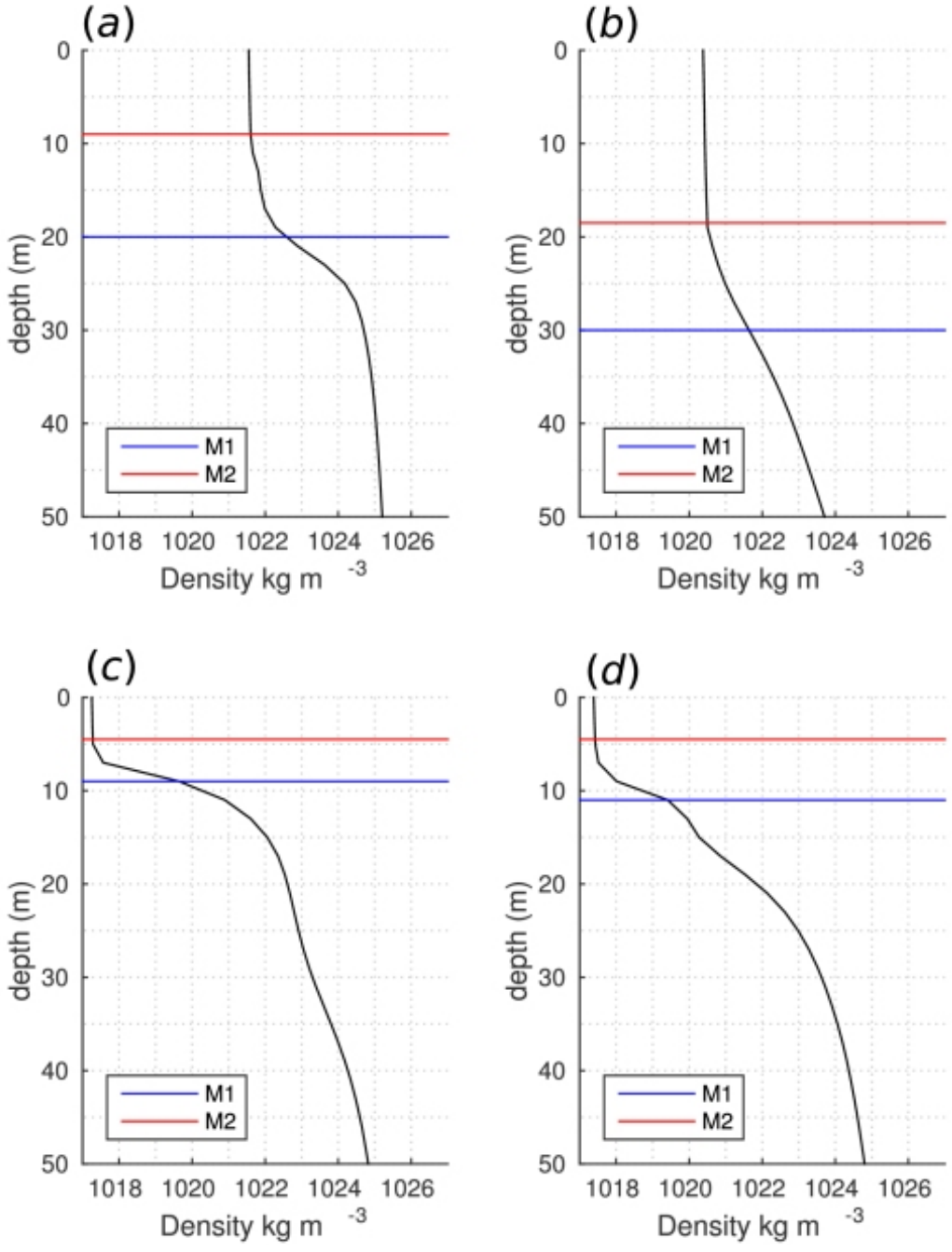

Fig 19: Different methods applied to simulated density profiles from a)ITP 1 winter b)ITP 43 winter c)ITP 1 summer d) ITP13 summer

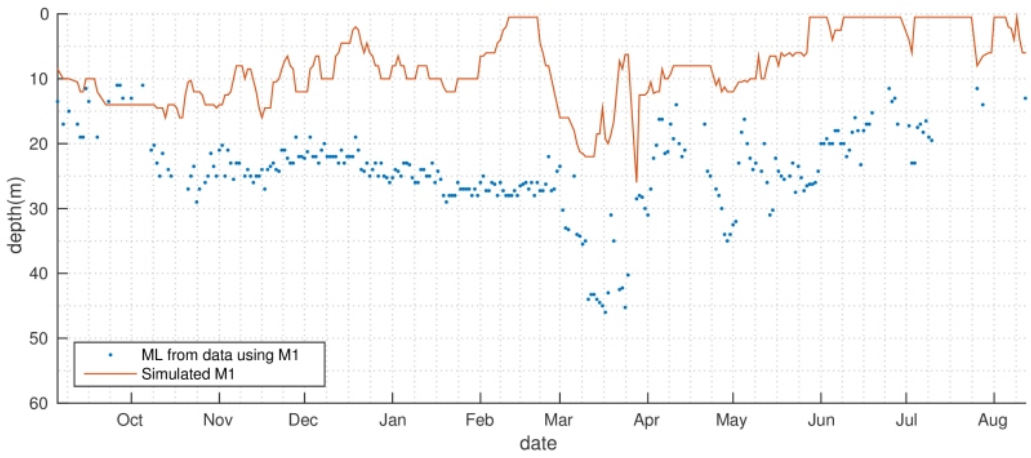

Fig 20: Mixed layer depth time series based on M1, simulation and data from ITP-62

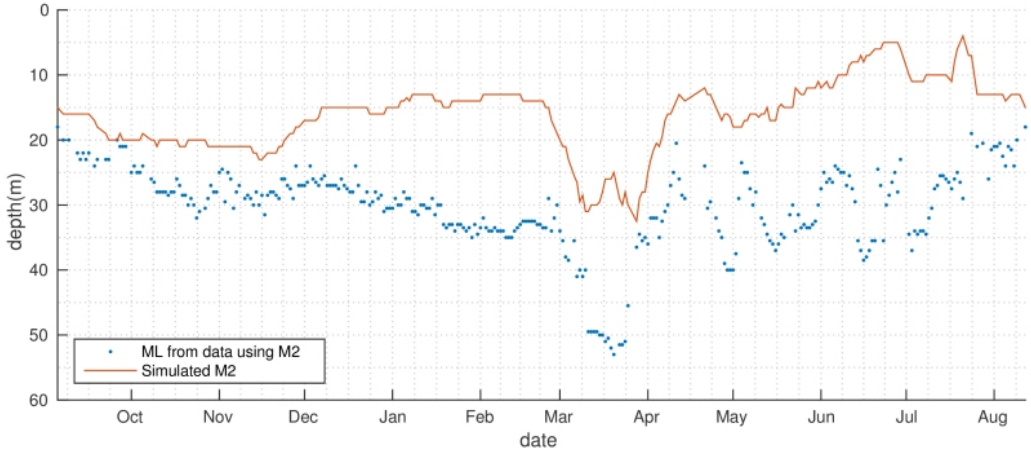

Fig 21: Mixed layer depth time series based on M2, simulation and data from ITP-62

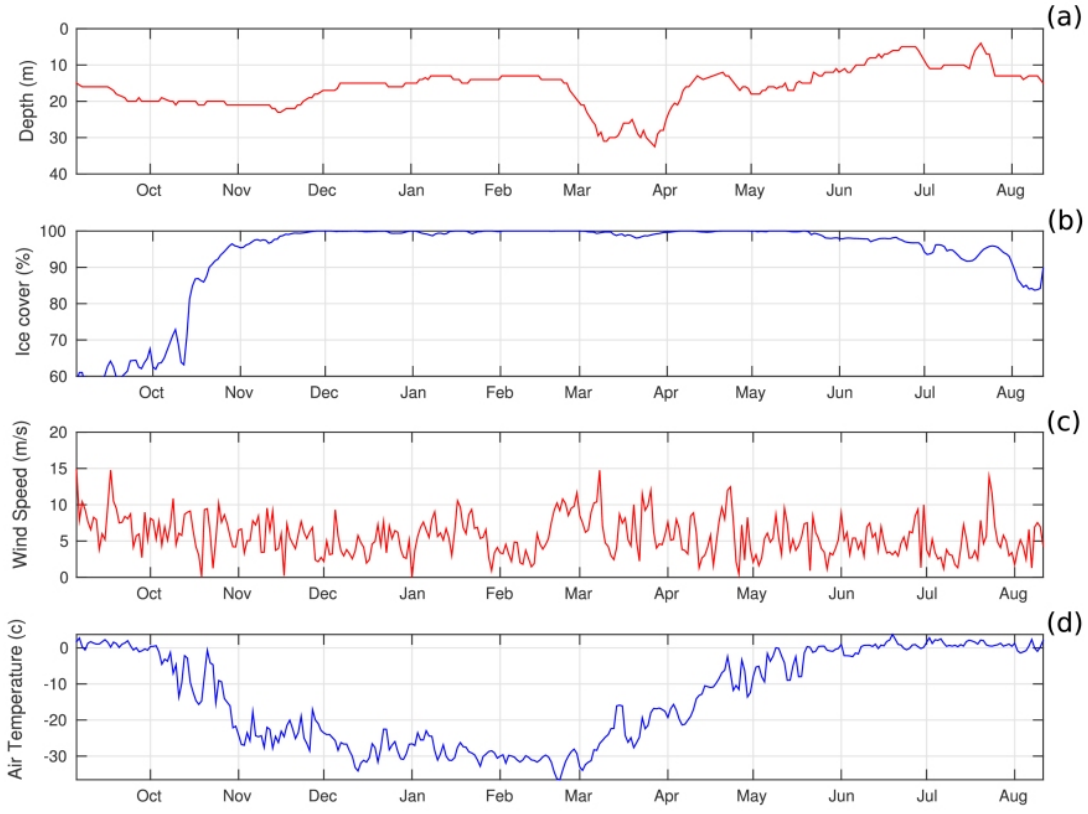

~~Fig 22: a) Mixed layer evolution during ITP 62 drift b) Sea-Ice fraction c) Wind Speed 10m above the surface d) Air temperature~~

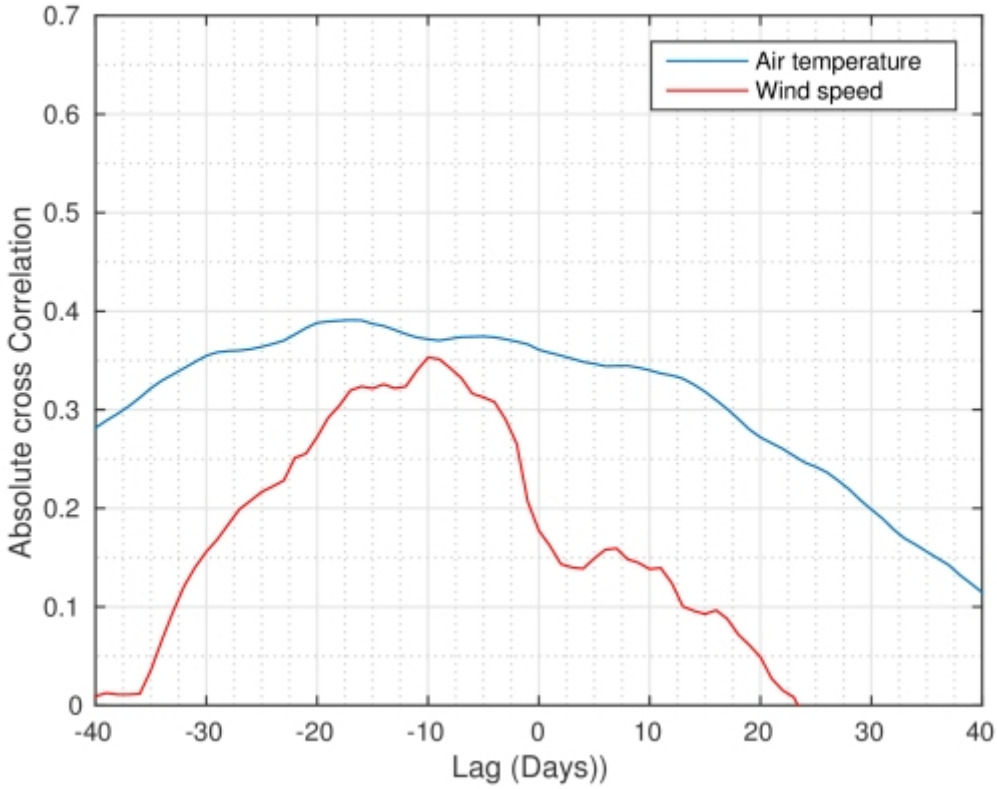

Fig 23: Cross Correlation of Mixed layer depth with wind speed and air temperature

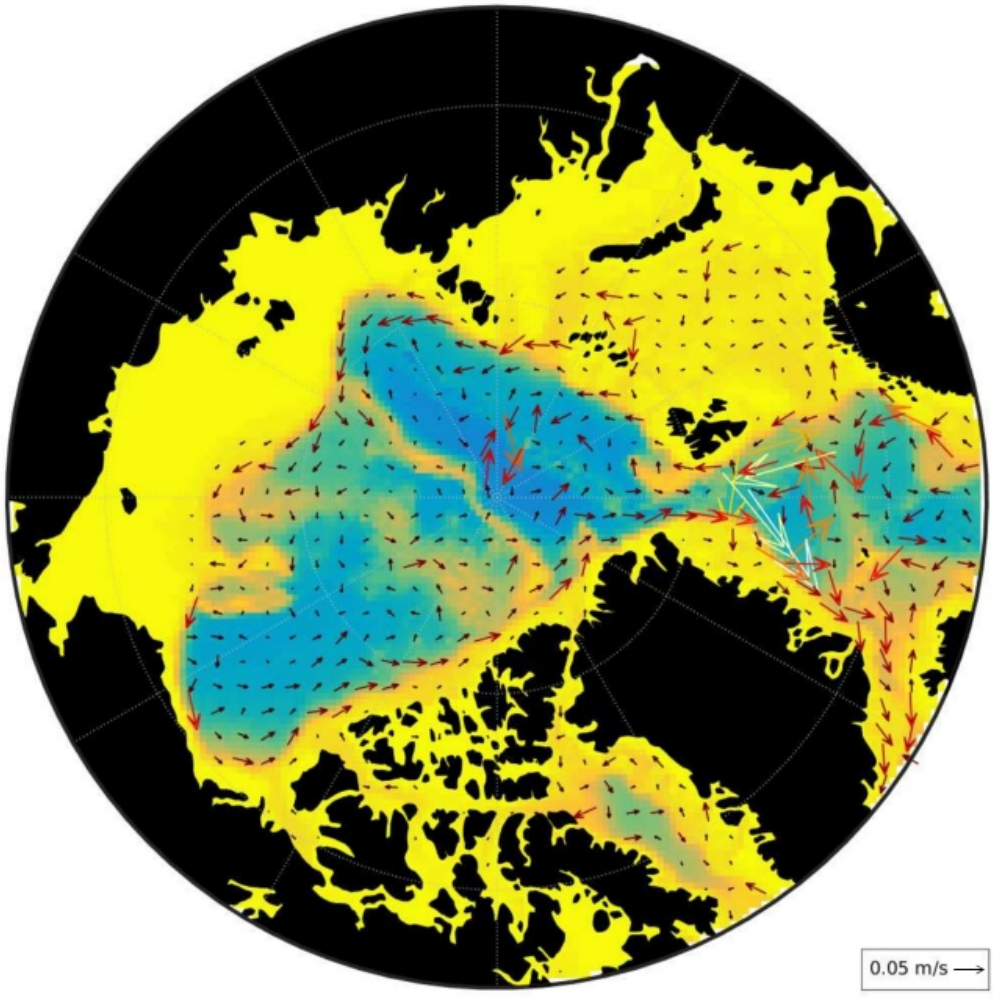

Fig 24. Model velocities averaged at 180-250(m) , 2006-2012

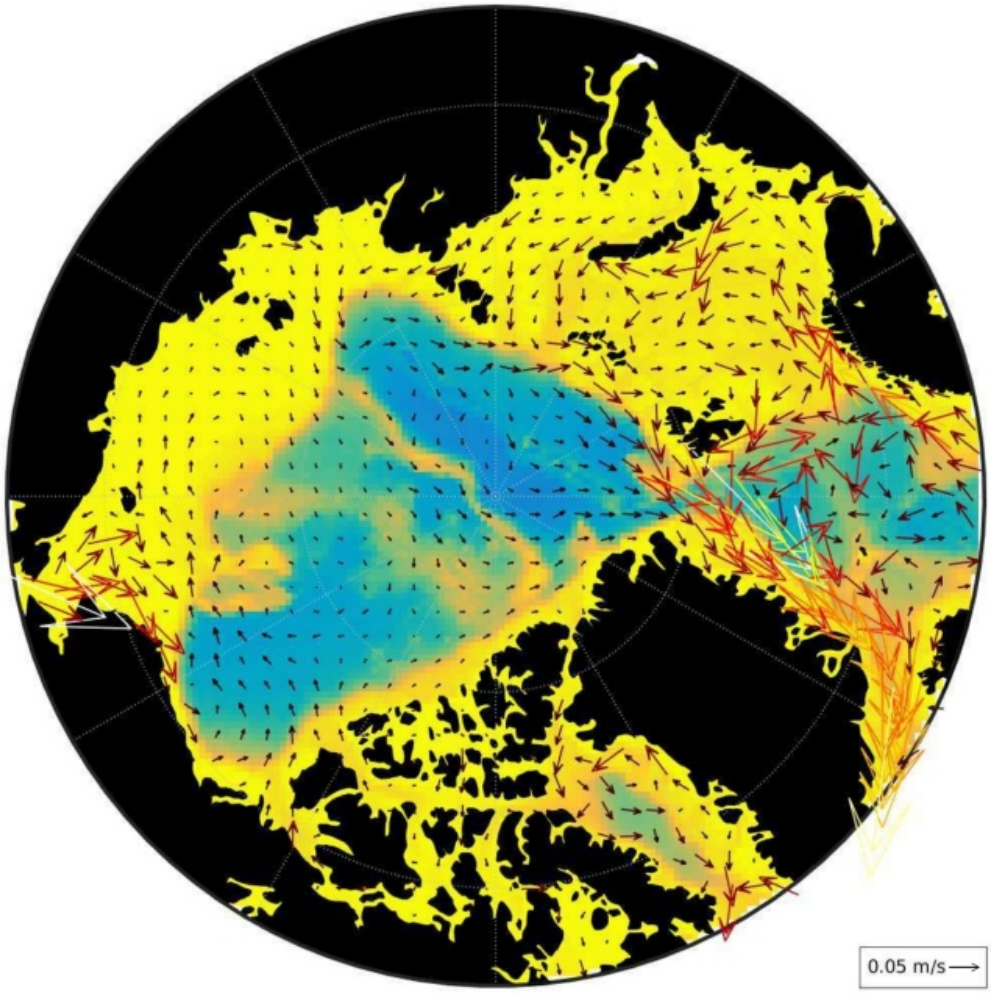

Fig 25. Model velocities averaged from 1-15 (m), 2006-2012

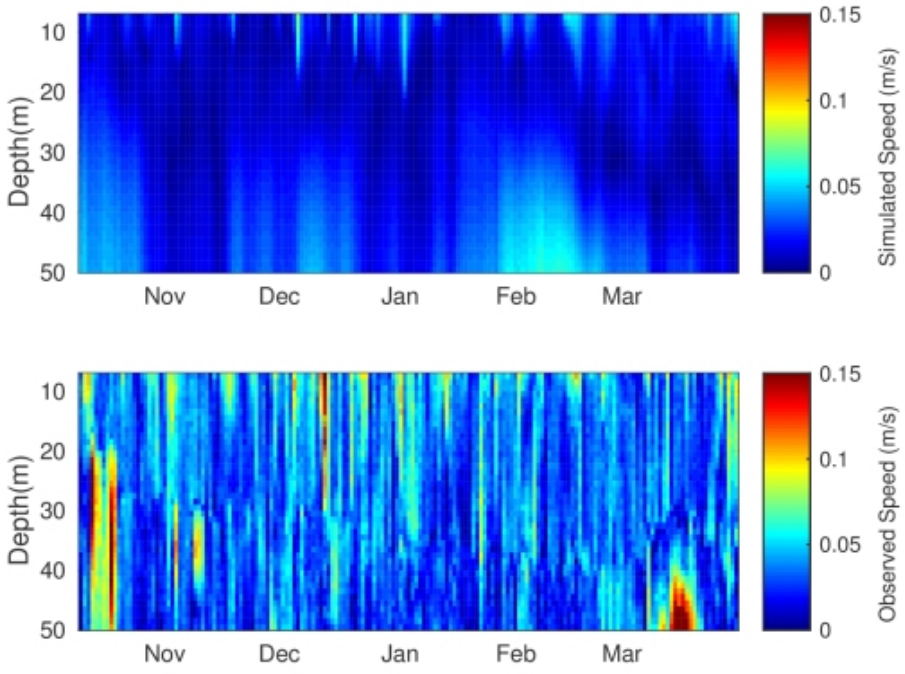

Fig 26. ITP-V Speed simulated and observed

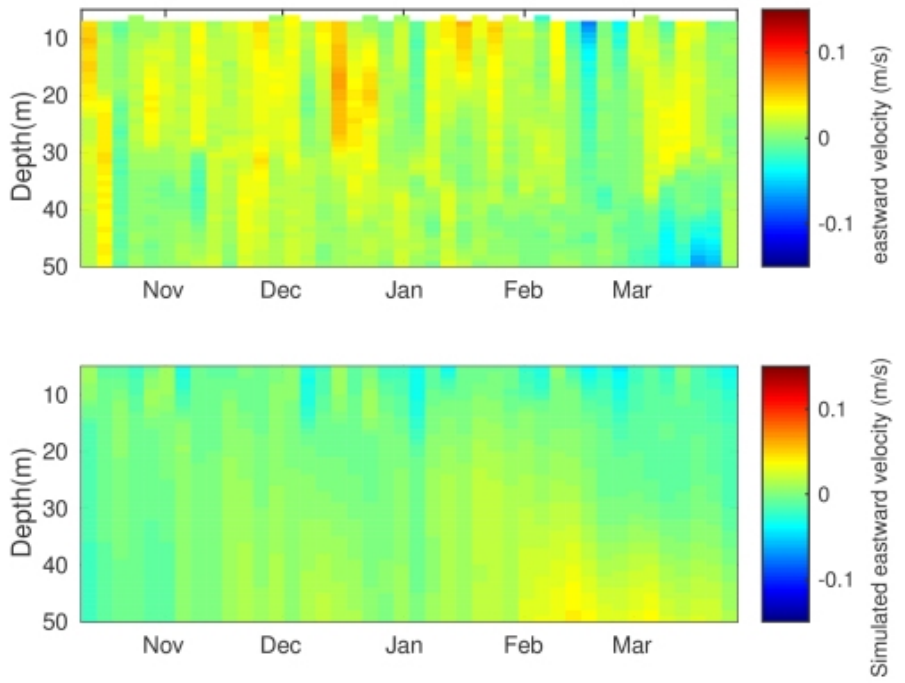

Fig 27. ITP-V Eastward velocity observed and simulated

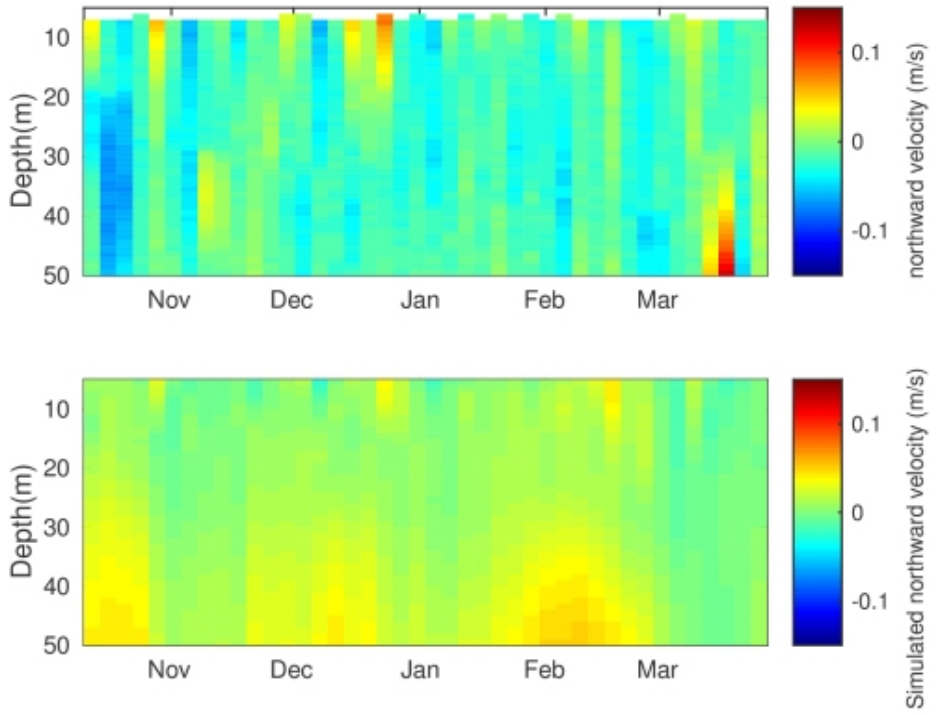

Fig 28. ITP-V Northward velocity observed and simulated

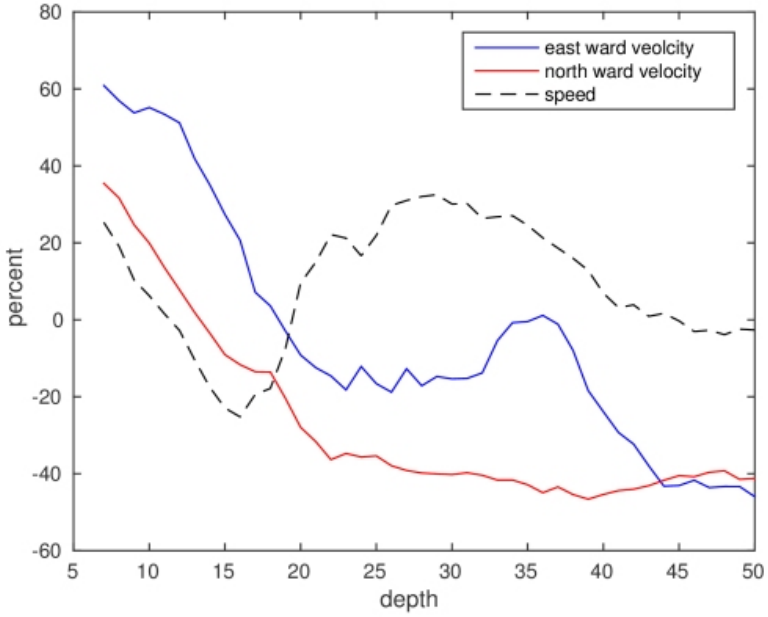

Fig 29. ITP-V correlation versus depth

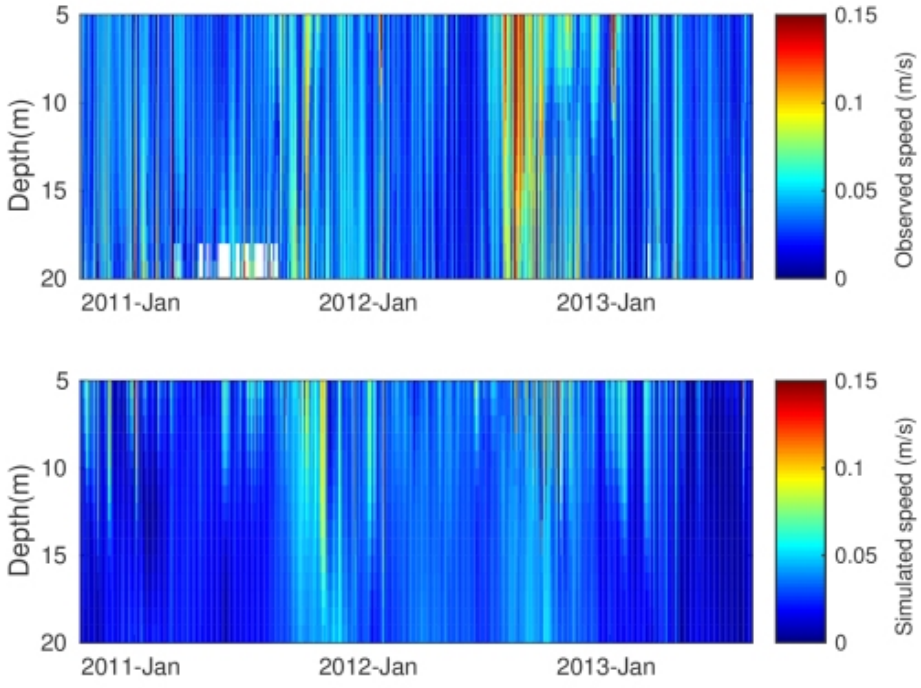

~~Fig 30. Mooring-D Observed and simulated Speed~~

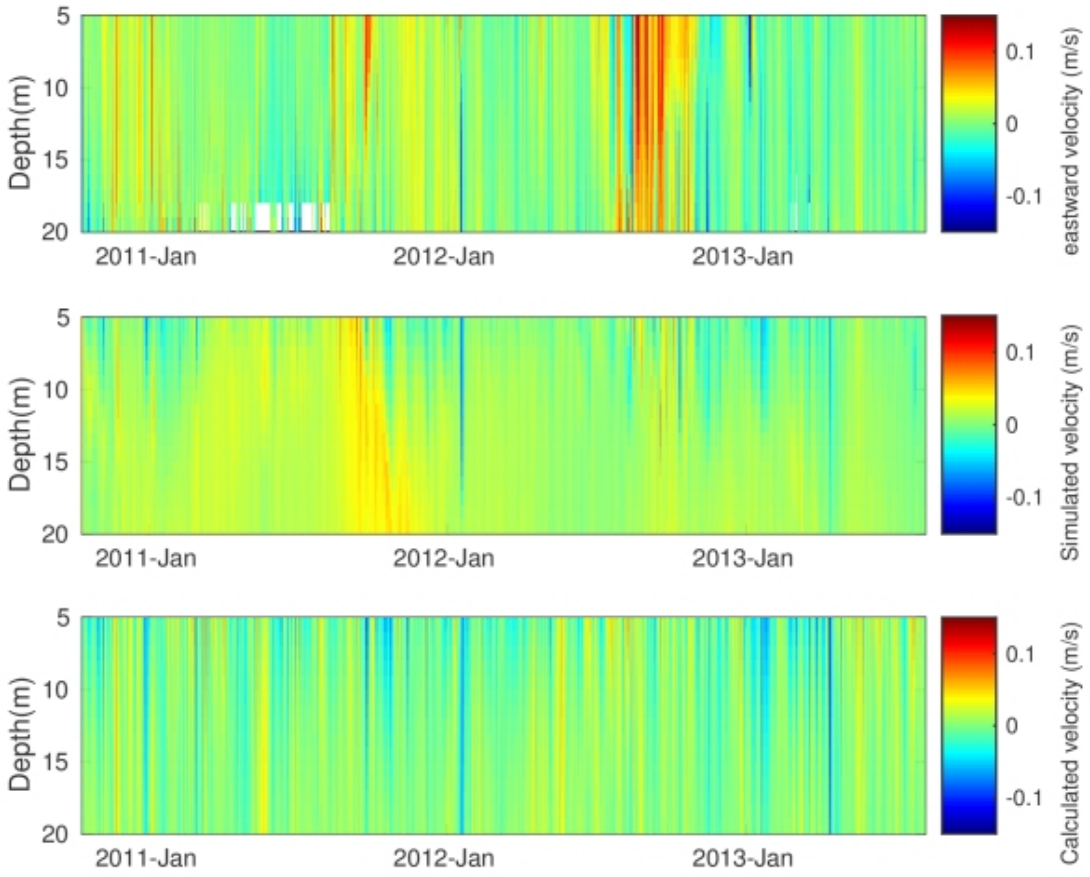

~~Fig 31. Mooring-D eastward velocity observed, simulated and estimated~~

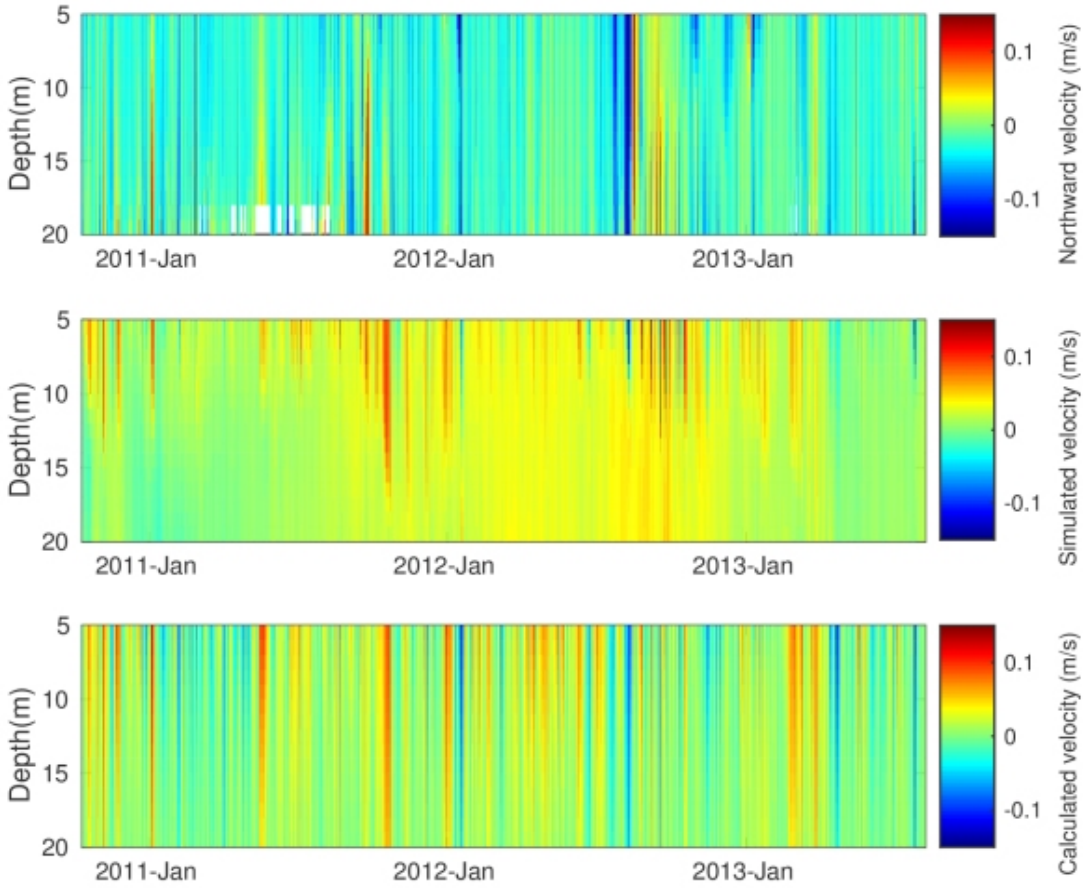

Fig 32. Mooring-D northward velocity observed, simulated and Estimated

Tables

	Sea ice fraction	**Sea ice drift**	**Sea ice velocity**	**Mixed layer depth**	**Water current velocity for back trajectory calculation**
Coarse resolution 3D simulation	Between 98% to 88% correlation	2 Km d^{-1} error	78% correlation	Model follows mixed layer evolution trend	29% correlation between model velocity and mooring data
Estimation from direct observation	Satellite data readily available	Remote sensing estimates available. Coverage is spotty.	Remote sensing estimates available. Coverage is spotty.	Mooring or ITP, but not available inside Lagrangian water parcel	Mooring or ITP, but not available inside lagrangian water parcel
Estimation from simple assumptions	No need for estimation	4.2 Km d^{-1} error	65% correlation	Not quantified	18% correlation between Ekman flow and mooring data.
Take home message	Use satellite data	Use satellite data where available. Model trajectories may have value as ensemble averages	Sea ice velocity from model has a good correlation and is valuable	Absolute value of MLD can be biased, but model can reveal the potential for changes	Ekman assumption is easier to implement, albeit less accurate by 11%. Simulations indicate a radius (10.3 km) for averaging properties.

Table 1 Summary of comparison between the simulation, estimation and data

Lett., **43**, 2016GL069671, doi:10.1002/2016GL069671.

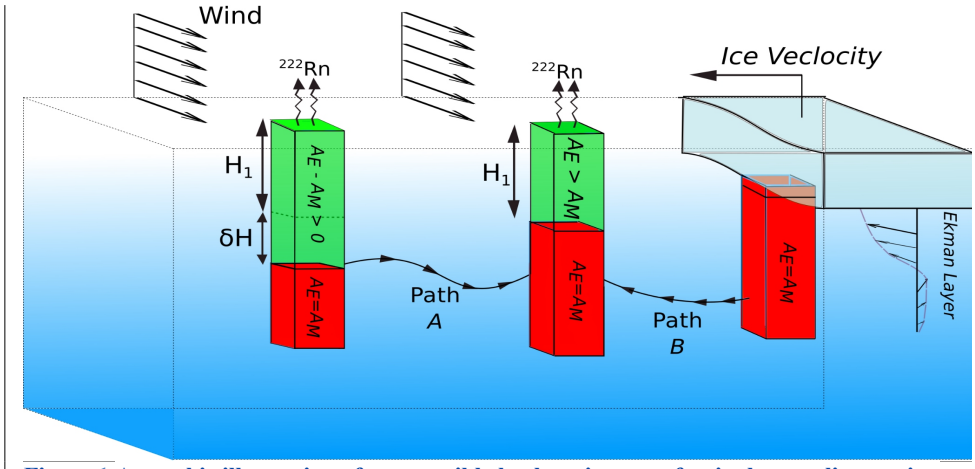

Figure 1 A graphic illustration of two possible back trajectory of a single sampling station

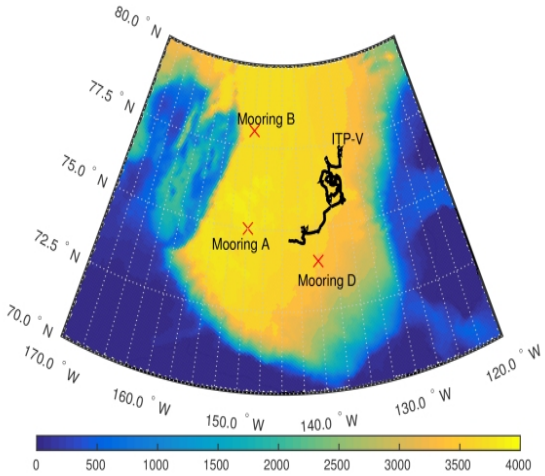

Figure 2: Bathymetry and location of ITP-V and Mooring for data comparison

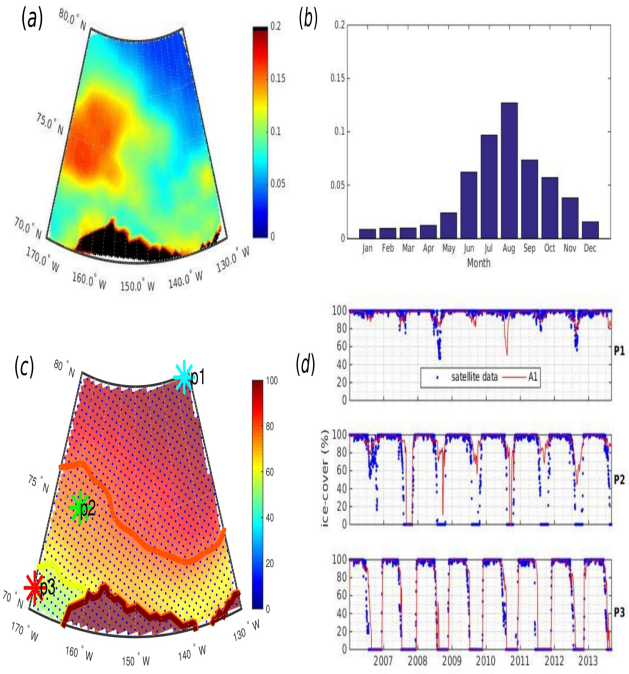

Figure 3 (A) Root mean square error averaged of A1 over time from 2006 to 2013; black mask covers the grid points on the ground. **(B)**Monthly averaged Annual Root Mean Square Error. **(C)** Averaged satellite sea ice cover from 2006-2013, Solid red line marking 80% cover and orange line marking 60%, Blue dots show the analysis grid, stars show the location of the three points Cyan P1, Green P2, Red P3 where time series data is graphed in D. **(D)**Time history of Sea-Ice fraction from top P1, P2 and P3, Satellite data compared with A1

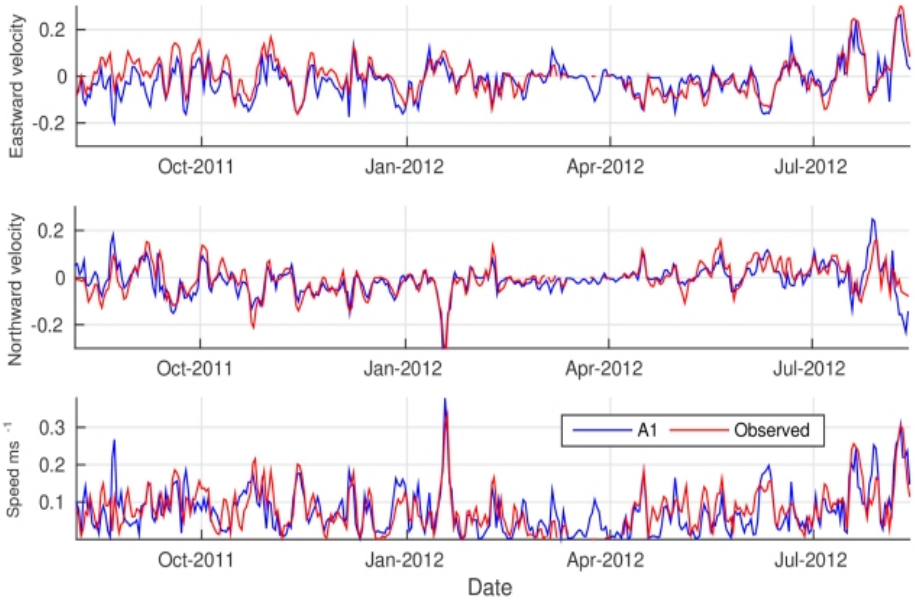

Figure 4: Time series of sea ice velocity components and speed of ITP 53 vs. 36 km horizontal resolution of MITgcm (A1). The correlations between eastward, northward and magnitude of velocity between ITP 53 data and A1 are 78%,75% and 80%, respectively.

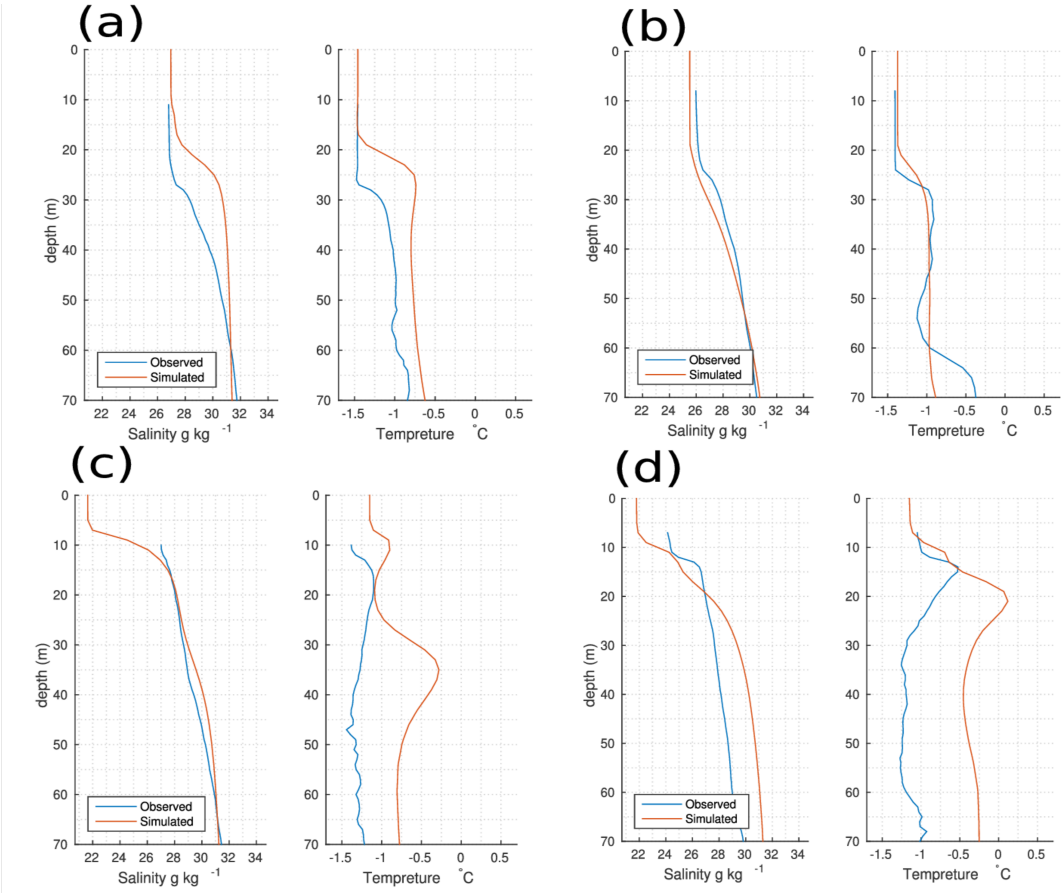

Figure 5 Salinity and Temperature of top 70 m based on ITPs and A1 **(a)** ITP 1 on 13-Dec-2006 at 74.80°N and 131.44°W **(b)** ITP-43 on 27-Nov-2010 at 75.41°N and 143.09°W **(c)**ITP 1 on 28-Aug-2006 at 76.96°N and 133.32°W **(d)** ITP-13 on 30-Jul-2008 at 75.00°N and 132.78°W

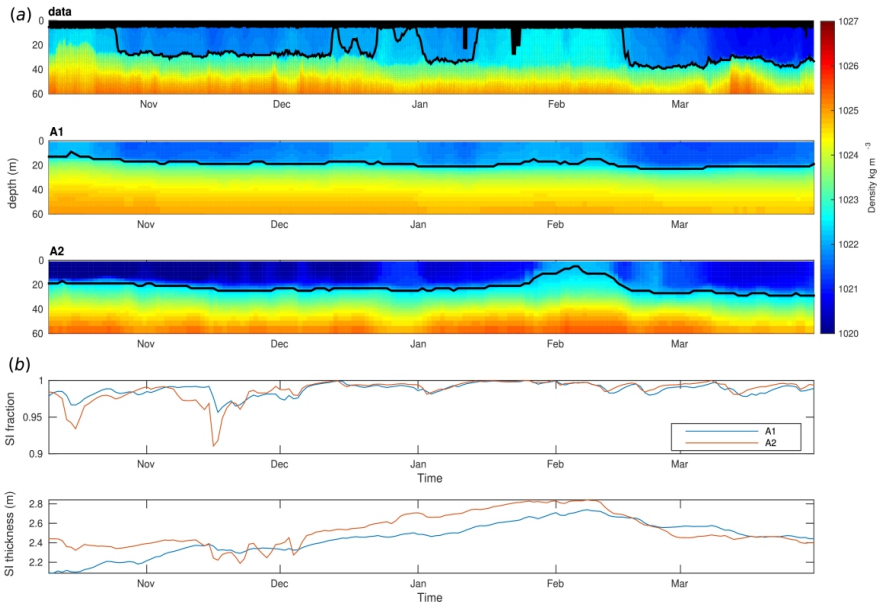

Figure 6 (a) Observed upper ocean density vs 36 km(A1) and 9 km(A2) resolution MITgcm density along the path of ITP drift, black mask covers areas that no data is available and solid black line shows isopycnal of 1022.5 . (b) Simulated sea ice fraction and thickness on top of the water column

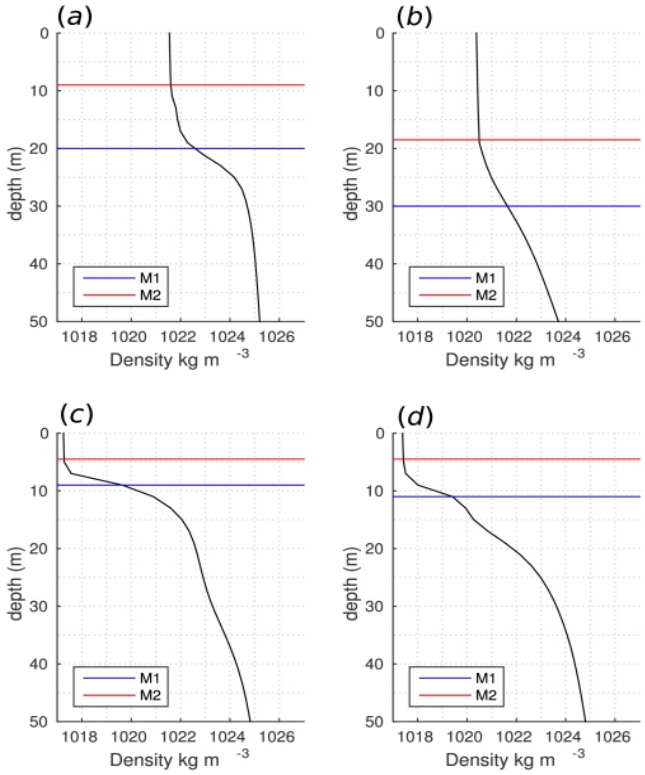

Figure 7 Methods M1 and M2 applied to selected ITP profiles

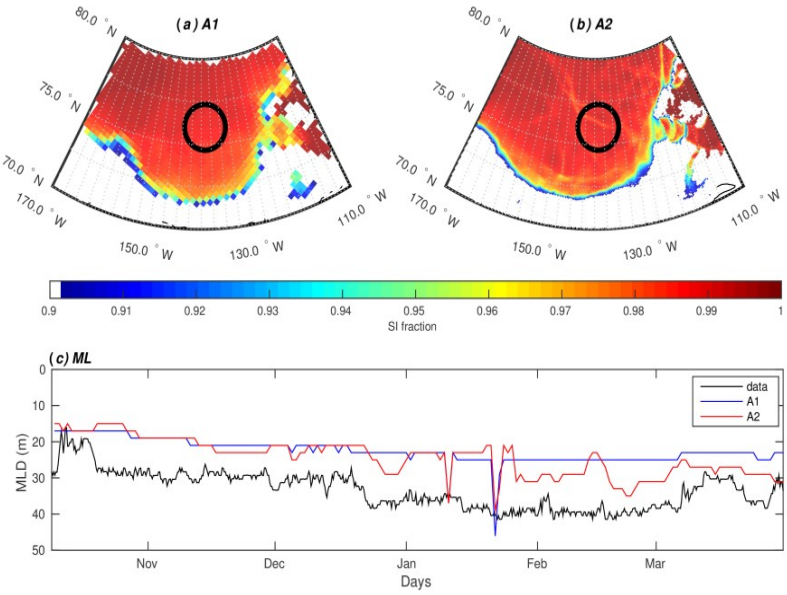

Figure 8 Sea ice cover higher than 0.9 with gray circle marking the area of ITP operation for **(a)** 36 km (A1) and **(b)** 9 km(A2) horizontal resolution of the model. A2 captured the ice opening and resulting mixed layer change while this phenomena has been averaged out by coarse resolution model **(c)** observed and simulated evolution of mixed layer depth on the path of ITP

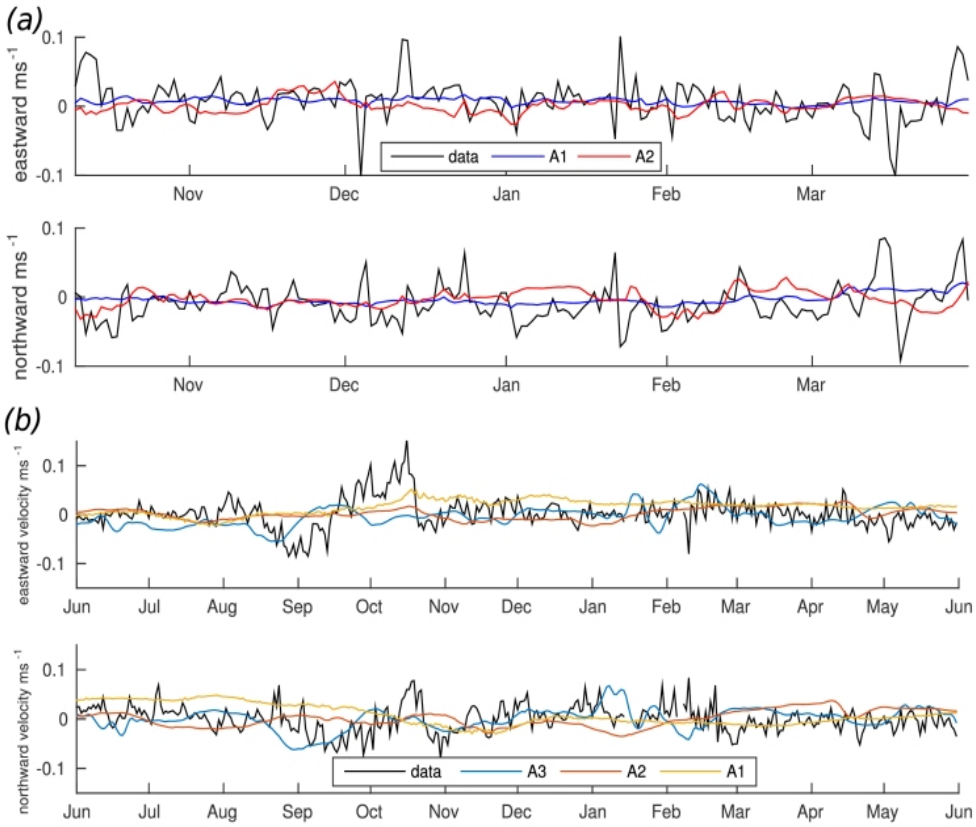

Figure 9 (a) Averaged velocity components from 5 to 50 meters observed by ITP-V vs simulated by A1 and A2 **(b)** Velocity components at 25 meters observed by mooring D vs A1,A2 and A3.

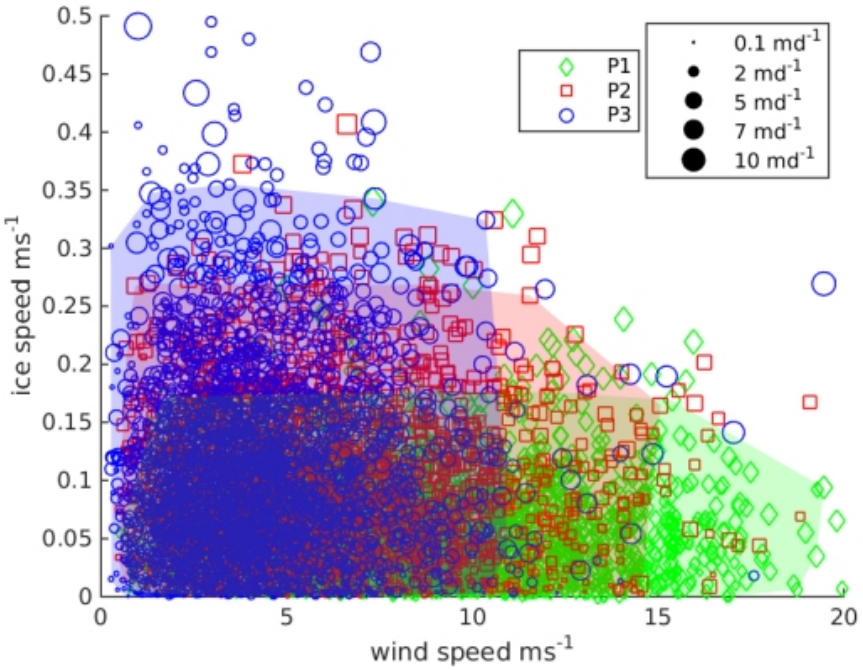

Figure 10 Gas exchange estimated vs wind and sea ice speed based on model outputs on grid points P1: 77.4N 143.6W, P2: 74.8N 163.5W and P3: 70.59N 159.4W from Jan-2006 to Dec-2012 , Areas enclose the outputs around the mean and two standard deviation. The size of the points demonstrate the magnitude of the gas exchange velocities normalized by sea ice cover.